

# The water balance representation in Urban-PLUMBER land surface models

H.J. Jongen<sup>1,2</sup>, M. Lipson<sup>3</sup>, A.J. Teuling<sup>1</sup>, C.S.B Grimmond<sup>4</sup>, J.-J. Baik<sup>5</sup>, M. Best<sup>6</sup>, M. Demuzere<sup>7,8</sup>, K. Fortuniak<sup>9</sup>, Y. Huang<sup>10</sup>, M.G. De Kauwe<sup>11</sup>, R. Li<sup>12,13</sup>, J. McNorton<sup>14</sup>, N. Meili<sup>15,16</sup>, K. Oleson<sup>17</sup>, S.-B. Park<sup>18</sup>, T. Sun<sup>12</sup>, A. Tsiringakis<sup>2,19</sup>, M. Varentsov<sup>20</sup>, C. Wang<sup>10,21</sup>, Z.-H. Wang<sup>22</sup> and G.J. Steeneveld<sup>2</sup>

<sup>1</sup>Hydrology and Environmental Hydraulics, Wageningen University, Wageningen, The Netherlands.

<sup>2</sup>Meteorology and Air Quality, Wageningen University, Wageningen, The Netherlands.

<sup>3</sup>Bureau of Meteorology, Canberra, Australia.

<sup>4</sup>Department of Meteorology, University of Reading, Reading, United Kingdom.

<sup>5</sup>School of Earth and Environmental Sciences, Seoul National University, Seoul, South Korea.

<sup>6</sup>Met Office, Exeter, United Kingdom.

<sup>7</sup>Urban Climatology Group, Department of Geography, Ruhr-University Bochum, Bochum, Germany.

<sup>8</sup>B-Kode, Ghent, Belgium.

<sup>9</sup>Department of Meteorology and Climatology, Faculty of Geographical Sciences, University of Łódź, Łódź, Poland.

<sup>10</sup>School of Meteorology, University of Oklahoma, Norman, Oklahoma, United States of America.

<sup>11</sup>School of Biological Sciences, University of Bristol, Bristol, United Kingdom.

<sup>12</sup>Institute for Risk and Disaster Reduction, University College London, London, United Kingdom.

<sup>13</sup>Department of Hydraulic Engineering, Tsinghua University, Beijing, China.

<sup>14</sup>European Centre for Medium-Range Weather Forecasts (ECMWF), Reading, United Kingdom.

<sup>15</sup>Department of Civil and Environmental Engineering, National University of Singapore, Singapore,

Singapore.

<sup>16</sup>Future Cities Laboratory Global, Singapore-ETH Centre, Singapore, Singapore.

<sup>17</sup>U.S. National Science Foundation National Center for Atmospheric Research (NSF NCAR), Boulder, Colorado, United States of America.

<sup>18</sup>School of Environmental Engineering, University of Seoul, Seoul, South Korea.

<sup>19</sup>European Centre for Medium-Range Weather Forecasts (ECMWF), Bonn, Germany.

<sup>20</sup>Faculty of Geography/Research Computing Center, Lomonosov Moscow State University, Moscow, Russia.

<sup>21</sup>Department of Geography and Environmental Sustainability, University of Oklahoma, Norman, Oklahoma, United States of America.

<sup>22</sup>School of Sustainable Engineering and the Built Environment, Arizona State University, Tempe, Arizona, United States of America

## Key Points:

- We evaluate the water balance in 19 urban land surface models (ULSM) from the Urban-PLUMBER project.
- ULSMs capture the timing of water fluxes more accurately than their magnitude.
- The water balance appears unclosed in 43% of the model runs (19 models at 20 sites).

---

Corresponding author: Harro Jongen, harro.jongen@wur.nl

**Abstract**

Urban Land Surface Models (ULSMs) simulate energy and water exchanges between the urban surface and atmosphere. When part of numerical weather prediction, ULSMs provide a lower boundary for the atmosphere and improve the applicability of model results in the urban environment compared with non-urban land surface models. However, earlier systematic ULSM comparison projects assessed the energy balance but ignored the water balance which is coupled to the energy balance. Here, we analyze the water balance representation in 19 ULSMs participating in the Urban-PLUMBER project using results for 20 sites spread across a range of climates and urban form characteristics. As observations for most water fluxes are unavailable, we examine the water balance closure, flux timing, and magnitude with a score derived from seven indicators. We find that the water budget is only closed in 57% of the model-site combinations assuming closure when annual total incoming fluxes (precipitation and irrigation) fluxes are within 3% of the outgoing (all other) fluxes. Results show the timing is better captured than magnitude. No ULSM has passed all good water balance indicators for any site. Our results indicate models could be improved by explicitly verifying water balance closure and revising runoff parameterizations. By expanding ULSM evaluation to the water balance and related to latent heat flux performance, we demonstrate the benefits of evaluating processes with direct feedback mechanisms to the processes of interest.

**Plain Language Summary**

Urban environments have their own local climates including typically higher nocturnal temperatures compared with rural areas. Ideally, modeling cities should capture their influences on the atmosphere above them. As the energy and water balances are linked by evaporation, a good water balance representation will support a good energy balance simulation. Focusing on the water balance, we find the water balance in models could be improved by paying attention to closure and runoff.

**1 Introduction**

The impact of urbanization on the local climate and hydrology has sparked scientists' interest and inspired research for centuries (e.g. Howard, 1833; Oke, 1982; Fletcher et al., 2013; Hamdi et al., 2020). With the increasing population in cities (United Nations, 2018) more people are impacted by increased heat stress and flooding (Heaviside et al., 2016; Gasparrini et al., 2017; Zhou et al., 2019; Botzen et al., 2020). Spatial morphological heterogeneity and human interactions make understanding the urban climate challenging (Kotthaus & Grimmond, 2014a; Sun et al., 2018; Koopmans et al., 2020; Demuzere et al., 2022), but weather and climate models need to include the effects of urban areas, as they locally exacerbate extreme events (Oleson et al., 2008; Ronda et al., 2017; Hertwig et al., 2020). Examples are increased flooding due to high impervious fractions (Zhou et al., 2019) and increased heat stress during heat waves resulting from the high heat storage capacity (Lemonsu et al., 2015). Therefore, models need to capture the impact of urban areas on their climate.

Researchers have developed, evaluated, and improved Urban Land Surface Models (ULSMs) simulating the interaction of the urban surface with the atmosphere. Coupled with a numerical weather prediction or climate model, ULSMs serve as a lower boundary condition and improve the model performance for urban environments (Tewari et al., 2007). ULSMs make different simplifying assumptions regarding urban geometry: a single homogeneous, impervious slab; multiple, individually homogeneous slabs; two-dimensional canyons; or 3D streets with individual buildings (Grimmond et al., 2009). These models also differ in whether and how they include physical processes like anthropogenic heat, irrigation, and snow processes (Lipson et al., 2023a). To evaluate their performance, these models are compared with observations (e.g. Ross & Oke, 1988; Grim-

mond & Oke, 2002; Hamdi & Schayes, 2007; Krayenhoff & Voogt, 2007; Porson et al., 2010). Although these individual evaluations were sometimes based on the same observations (Grimmond et al., 2009), the lack of a systematic approach prevented consistent comparison of the schemes. To compare the wide variety of models, two successive comparison projects applied a systematic approach. The first systematic comparison of ULSMs generally followed the PILPS protocol (project for intercomparison of land surface parameterization schemes, Henderson-Sellers et al. (1996)), hence PILPS-Urban (Grimmond et al., 2010, 2011). Individual modelers received meteorological input and surface characteristics to enable them to run their models. In total, 32 models completed simulations for a site in Vancouver and one in Melbourne. Grimmond et al. (2011) concluded that increased model complexity did not necessarily benefit model performance.

The second intercomparison, Urban-PLUMBER (Lipson et al., 2023a), assesses 30 models initially at the PILPS-Urban Melbourne site and adopts benchmarks following the PLUMBER project (Best et al., 2015). Benchmarks serve as a relative reference, to which models are compared to assess whether a cohort performs better (or not) than the benchmark and if input information is utilized effectively. Urban-PLUMBER is extended to the 20 sites presented by Lipson et al. (2022a) in the second phase (Lipson et al., 2023b). The Urban-PLUMBER models outperform the PILPS-Urban ones for the sensible and latent heat flux. Some models representing two-dimensional canyons now perform nearly as well as one and two-tile models after efforts to improve hydrology and vegetation representation. However, models with complex urban geometry often still have relatively simple hydrology and vegetation and perform less well overall (Lipson et al., 2023a). Suggesting the representation of hydrology and vegetation requires more attention (Lipson et al., 2023a).

Although PILPS-Urban and Urban-PLUMBER conclude vegetation and hydrology are important for model performance, neither project evaluates the water balance explicitly. The water balance satisfies the conservation of mass (Lavoisier, 1789) in the same way the energy balance satisfies the conservation of energy (Châtelet, 1740). The conservation of energy is forced in many ULSMs to prevent the energetic state of the model from drifting and the consequential, long-term bias in the modeled surface fluxes (Grimmond et al., 2010). Closure is achieved by either updating the surface temperatures based on the residual energy or restricting the turbulent heat flows to the available energy (Grimmond et al., 2010). Both PILPS-Urban and Urban-PLUMBER test whether models close the energy balance, but have not verified the numerical closure of the water balance. Similar to the energy balance, an unclosed water balance can result in model biases and consequential drifting. These biases may in turn affect the energy balance, as the energy and water balance are linked through evapotranspiration ( $ET$ ), the mass counterpart of the latent heat flux ( $Q_E$ ). This direct link implies errors and/or biases in one balance will affect the model's skill for the other balance. Recently, Yu et al. (2022) showed the hydrology in a coupled ULSM has the potential to improve the  $Q_E$ , humidity, and air temperature with impacts up into the boundary layer ( $\sim 1$  km).  $ET/Q_E$  has been amongst the most challenging fluxes for ULSMs from the first assessment (Ross & Oke, 1988) until now (Grimmond et al., 2011). Given the link to the energy balance, closing the water balance may improve model performance for the energy balance fluxes.

However, the water balance cannot be directly assessed because of a lack of observations at the appropriate spatiotemporal scales at this time. While precipitation is measured routinely in many urban locations with rain gauges and rain radars, runoff, irrigation, and changes in water storage are not.  $Q_E$  ( $ET$ ) observations from eddy-covariance systems have substantial gaps introduced in the quality control process (Feigenwinter et al., 2012) that rejects more data close to rain events (Grimmond, 2006). Runoff is occasionally measured in urban catchments (Berthier et al., 1999; Walsh et al., 2005), but a challenge is posed by the difference in the source area of observations for runoff and eddy-covariance techniques (Grimmond & Oke, 1986, 1991; Hellsten et al., 2015). Ex-

145 ternal water use, often irrigation, further complicates the water balance in cities, as it  
 146 mainly occurs at the micro-scale (e.g. garden irrigation). This scale can only be inferred  
 147 from neighborhood piped water supply observations and water use surveys or estimated  
 148 from weather, vegetation, and soil type (Grimmond & Oke, 1986; Mitchell et al., 2001;  
 149 Zeisl et al., 2018; Kokkonen et al., 2018). Tree roots penetrate (sewer) pipes causing dam-  
 150 age (Randrup et al., 2001) and simultaneously taking out water, which is an unobserved  
 151 term. Lastly, measuring the water storage change is logistically difficult, as this requires  
 152 the state of each individual element contributing to water storage in the city, such as soil  
 153 moisture, interception, groundwater, and surface water. Thus, a direct comparison of a  
 154 full set of water balance observations is extremely challenging and an alternative approach  
 155 is needed.

156 Here, we develop an alternative approach to evaluate the representation and dy-  
 157 namics of the water balance in ULSMs. To examine the water balance closure, we pro-  
 158 pose an UWBR (urban water balance representation) score. The score combines seven  
 159 indicators assessing: water balance closure (1 indicator),  $ET$  (2), water storage dynam-  
 160 ics (2), and surface runoff (2). The UWBR score is applied, given a lack of observations,  
 161 to rank models' capability to accurately capture different aspects of the water balance.  
 162 Assessing the score of 19 Urban-PLUMBER ULSMs with a complete water balance rep-  
 163 resentation helps to identify model improvement possibilities. The water balance rep-  
 164 resentation is compared with the turbulent heat fluxes model skill since we expect a bet-  
 165 ter water balance representation should improve simulated latent heat fluxes.

## 166 2 Methods

### 167 2.1 Urban water balance representation (UWBR) score

168 The UWBR score is a linear sum of seven indicators of a good water balance, which  
 169 are assigned a value of 1 if a specified threshold is passed (Table 1), except the  $I_{S,m}$  in-  
 170 dicator, for which both sub-metrics are assigned 0.5 if passed. No weights are assigned,  
 171 as these cannot be determined objectively. The UWBR score is compared with the model  
 172 performance for the latent heat flux assessed with metrics capturing different character-  
 173 istics (Willmott, 1982) that are not entirely independent:

- 174 • Absolute mean bias error ( $|MBE|$ ) assesses the bias providing insight into how well  
 175 the quantities of the latent heat flux are modeled.
- 176 • Coefficient of determination ( $R^2$ ) captures the consistency of the timing as  $R^2$  de-  
 177 creases with a shift in a quasiperiodic signal like the latent heat flux.
- 178 • Normalized standard deviation ( $\sigma_{norm}$ ,  $\sigma_{model}$  divided by  $\sigma_{observations}$ ) compares  
 179 the variability, which is dominated by the daily cycle in the case of the latent heat  
 180 flux.
- 181 • Systematic Mean Absolute Error ( $MAE_s$ ) indicates the average error. The sys-  
 182 tematic error is separated from the unsystematic error similarly to the approach  
 183 presented by Willmott (1982) for the root mean square error. This separation al-  
 184 lows us to distinguish between systematic and random errors.
- 185 • Unsystematic Mean Absolute Error ( $MAE_u$ ) assesses how well the erratic behaviour  
 186 is captured.

187 Before the individual indicators are introduced, we define two ways to calculate wa-  
 188 ter storage from the model output based on either the water storage term or the other  
 189 terms of the water balance combined. Assuming that the net change in water stored in  
 190 a "catchment" or a model grid ( $\Delta S$ ) can be derived from the difference between the in-  
 191 coming and outgoing water fluxes, then:

$$192 \quad \Delta S = P + I - (R + ET) \quad (1)$$

193 where  $P$  is precipitation,  $I$  irrigation, and  $R$  runoff.  $R$  represents both the surface ( $R_s$ )  
 194 and the subsurface ( $R_{sub}$ ) runoff. When  $\Delta S$  is calculated from the fluxes on the right-  
 195 hand side of Eq. 1, we refer to this as the net water flux. Following the urban water bal-  
 196 ance (Grimmond & Oke, 1986), the net storage change ( $\Delta S$ ) should account for the wa-  
 197 ter storage change above and below ground, such as the interception, water bodies, and  
 198 groundwater. The components actually included depend on the model conceptualization.  
 199 Here, we refer to the storage represented in the model as the water storage ( $\Delta S_{model}$ ):

$$200 \quad \Delta S_{model} = \Delta S_{soil} + \Delta S_{intercept} + \Delta S_{snow} \quad (2)$$

201 where  $\Delta S_{soil}$  is storage change in the soil moisture,  $\Delta S_{intercept}$  storage change in  
 202 the interception storage, and  $\Delta S_{snow}$  storage change in the snow cover. When we refer  
 203 to annual timescales, the analysis is performed on all time intervals of a year in the time  
 204 series, i.e. a new annual period starts at every timestep, after which a full year of data  
 205 is available (e.g. NL-Amsterdam: 2018-05-01 19:00 - 2019-05-01 19:00, 2018-05-01 20:00  
 206 - 2019-05-01 20:00, etc.). This method maximizes the use of available data and elimi-  
 207 nates the influence of choosing a specific annual period like the calendar or hydrologi-  
 208 cal year.

### 209 **2.1.1 Water balance closure**

210 Water balance closure assumes that all fluxes add up to zero for the time and space  
 211 under consideration (here  $\sim 1 \text{ km}^2$  and one year):

$$212 \quad P + I - (R + ET + \Delta S) = 0 \quad (3)$$

213 where  $\Delta S$  corresponds to the water storage in the model (Eq. 2) to prevent closure re-  
 214 sulting from calculating the storage change based on the fluxes. Three models (8, 16, and  
 215 17) model groundwater interaction, which is not included in the model output. We ex-  
 216 amine the annual water balance closure with the annual total fluxes normalized by an-  
 217 nual precipitation plus irrigation to enable comparison between sites with a range of pre-  
 218 cipitation regimes.

219 The water balance closure indicator ( $I_A$ , Table 1) assesses if the total sum of all  
 220 fluxes (including storage) is less than 3% from  $P + I$ . The 3% threshold allows for non-  
 221 closure due to unsaved interception storage data not being provided in the model out-  
 222 put, errors arising in latent heat flux unit conversion, or numerical model errors. Inter-  
 223 ception storage is represented in all 19 models analyzed here, but only three model out-  
 224 puts provided the values. According to the literature, this may explain a non-closure of  
 225 up to 0.5% (Klaassen et al., 1998; Wouters et al., 2015; Carlyle-Moses et al., 2020). Con-  
 226 version of latent heat flux to  $ET$  can vary by up to 2% depending on temperature and  
 227 snow effects (Bringfelt, 1986; Petrucci et al., 2010). Not all models correct for these ef-  
 228 fects. To account for numerical model errors arising from discretization and time step-  
 229 ping (MacKay et al., 2022), we allow deviations of up to 0.5%.

### 230 **2.1.2 Evapotranspiration (ET)**

231 The two  $ET$  indicators address the magnitude and timing. Given gaps in  $ET$  ob-  
 232 servations prevent direct comparison of total modeled  $ET$  ( $ET_{model}$ ) over a model pe-  
 233 riod, we use one of the Lipson et al. (2023a) benchmark models. This allows a total  $ET$   
 234 to be obtained without gaps. The Lipson et al. (2023a) benchmark model ( $ET_{bench}$ ) is  
 235 derived using multivariate ordinary least squares regressions with a K-means clustering  
 236 approach. The K-means clustering approach is trained in-sample using 81 clusters on  
 237 four variables: incoming shortwave radiation, air temperature, relative humidity, and wind  
 238 speed (KM4-IS-SWdown-Tair-RH-Wind in Lipson et al., 2023a). To reduce the hourly  
 239 MBE, wind speed is omitted at both Helsinki sites. At all sites, the MBE is below  $1 \text{ W m}^{-2}$   
 240 and at most sites below  $0.1 \text{ W m}^{-2}$  evaluated against available data.

**Table 1.** Overview of the seven indicators that are linearly combined in the UWBR score, which is used to evaluate the urban water balance representation in ULSMs. The criterion indicates what needs to be achieved to assign a value of 1 to the indicator or 0.5 per test in the case of  $I_{S,m}$ . The uncertainty criteria (\*) are discussed in sections 2.1.2 and 2.1.4. The notation in the equations is defined in the corresponding subsections of section 2.1. The details on all indicators can be found in section 2.1.

<b>Water balance flux</b>	<b>Indicator</b>	<b>Description</b>	<b>Criterion</b>	<b>Equation</b>
All	$I_A$	Closure of the annual water balance assessed relative to the precipitation plus irrigation	$< 0.03$	$\left  \frac{P+I-(R+ET+\Delta S)}{P+I} \right $
ET	$I_{ET,m}$	Modeled cumulative $ET$ normalized by the benchmark $ET$ ( $ET_{bench}$ ) over the whole model period	Within benchmark uncertainty*	$\frac{ET_{model}}{ET_{bench}}$
	$I_{ET,t}$	Similarity of $ET$ recession timescale distribution between model and observations from the whole model run	$p < 0.05$	Kolmogorov-Smirnov test (Chakravarti et al., 1967)
$\Delta S$	$I_{S,m}$	Range over the whole model run in stored water derived from the modeled water storage and the net water flux compared to water storage capacity	$< (50\% \text{ of soil volume} + 3 \text{ mm interception})$	Range in cumulative $\Delta S_{model}$ (Eq. 2) and $\Delta S$ (Eq. 1)
	$I_{S,t}$	Coefficient of determination ( $R^2$ ) between changes in modeled water storage and the net water flux over the whole model period	$> 0.9$	$R^2$ of changes in $\Delta S_{model}$ (Eq. 2) and changes in $\Delta S$ (Eq. 1)
$R_s$	$I_{R,m}$	Curve number ( $CN$ ) from modeled runoff events and from site characteristics	Within $CN$ uncertainty*	$CN$ method (section 2.1.4)
	$I_{R,t}$	Mean lag (hours) between center of mass from precipitation and surface runoff of all events	$< 1 \text{ hour}$	$R_{s,centroid} - P_{centroid}$

Therefore,  $ET_{bench}$  is assumed to provide a reasonable estimate of the total  $ET$  flux over the model run for the  $I_{ET,m}$  indicator (Table 1). We compare in  $Q_E$  units rather than  $ET$ , eliminating unit conversions and calculate the cumulative  $ET$  flux uncertainty from the benchmark based on (1) the benchmark MBE multiplied by the run duration, and (2) lack of energy balance closure associated with eddy-covariance observations (Franssen et al., 2010; Foken et al., 2012; Mauder et al., 2020). The lack of energy closure is calculated by the net all-wave radiation minus the sum of the turbulent heat fluxes. If a lack of closure occurs, the unexplained energy is split between  $Q_E$  and  $Q_h$  on the Bowen ratio (Twine et al., 2000; Hirschi et al., 2017; Mauder et al., 2020). The  $Q_E$  share is combined with the MBE multiplied by the run duration to form the benchmark uncertainty yielding a maximum uncertainty, as some energy will go to the storage heat flux. A model run passes  $I_{ET,m}$  when  $ET_{model}$  falls within the uncertainty of  $ET_{bench}$ .

The timing of modeled  $ET$  is assessed assuming exponential  $ET$  recession after rainfall based on the recession timescale estimated following the Jongen et al. (2022) methodology. This methodology considers only the first ten days to exclude the influence of longer dry periods and irrigation. A daily-timescale analysis circumvents observational gaps. Model and observations are assessed if they have the same distribution for the recession timescale with a Kolmogorov-Smirnov test (Chakravarti et al., 1967). The  $I_{ET,t}$  indicator is assigned a value of 1 when the p-value is below 0.05.

### 2.1.3 Water storage

Indicator  $I_{S,m}$  evaluates the water storage by comparing the modeled water storage and cumulative net water flux ranges (Section 2.1) over the analysis period with respect to the estimated water storage capacity. According to the literature, soil water storage capacity is maximally half the soil depth for all soil types (Saxton et al., 1986). As the modeled soil depth depends on the model run, the soil water storage capacity is calculated for each separately. To account for interception storage, 3 mm is added to the estimated water storage capacity based on tree and impervious interception observations (Klaassen et al., 1998; Wouters et al., 2015; Carlyle-Moses et al., 2020). The two models not including soil moisture do not pass the first check of this indicator and are only evaluated based on the net water flux (Table 2). Other models receive 0.5 score when either the modeled water storage range or the net cumulative water flux range falls within the estimated water storage capacity (or 1 for both).

Indicator  $I_{S,t}$  quantifies the internal temporal consistency between the change in water storage (Eq. 2) and the net water flux (Eq. 1), which should be indicating the same flux. The coefficient of determination  $R^2$  (Willmott, 1982) is calculated using storage changes using 30-min (or 60-min) model output depending on the site forcing data. This metric equals 1 if the timing between two fluxes is similar ( $R^2 > 0.9$ ) independent of the flux bias, unlike other indicators (e.g.  $I_A$ ). The two models without soil moisture output are assigned a value of 0 for  $I_{S,t}$  as their performance could not be evaluated.

### 2.1.4 Surface runoff ( $R_s$ )

Indicator  $I_{R,m}$  assesses the  $R_s$  magnitude relating total event precipitation to  $R_s$  (Figure 1a). Without runoff observations, curve numbers ( $CN$ ) are derived to evaluate modeled total event  $R_s$  (Cronshey et al., 1985) based on the relation between the total event precipitation ( $P_e$ ) and the total event  $R_s$  ( $R_e$ ):

$$R_e = \frac{(P_e - 0.2S)^2}{P_e + 0.8S} \text{ with } S = \frac{1000}{CN} - 10 \quad (4)$$

where  $S$  is the potential maximum retention. To determine when precipitation events are independent, the auto-correlation of precipitation events is examined. A dry period of five hours (Figure S1) is assumed across all sites, which is consistent with Wenzel Jr

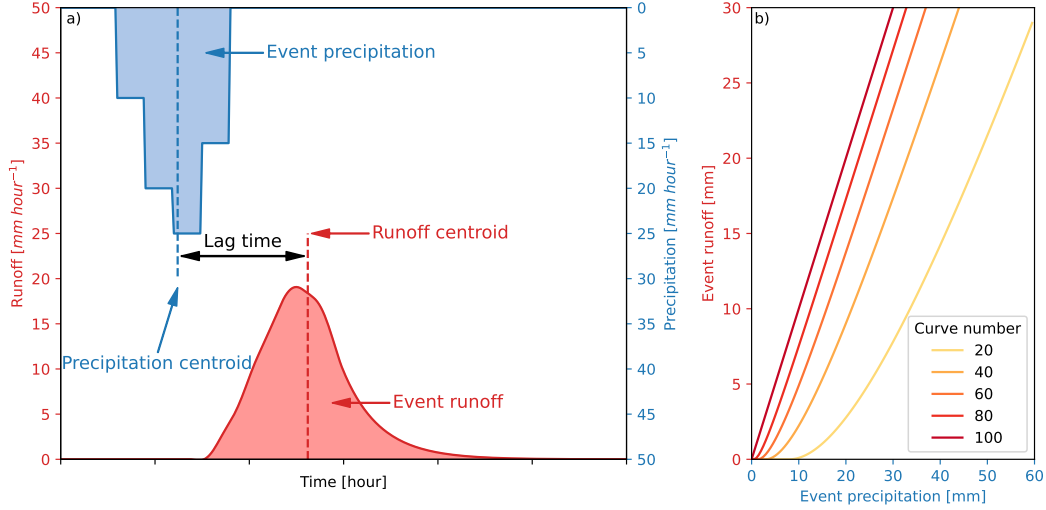


**Figure 1.** Illustration of surface runoff indicators ( $I_{R,m}$  and  $I_{R,t}$ ) showing (a) lag time between an event precipitation centroid and surface runoff centroid, and (b)  $CN$  values (Eq. 4) derived from total event precipitation and surface runoff.

289 and Voorhees (1981). To exclude snow events, the analysis includes only events with a  
 290 minimum air temperature above  $0^{\circ}\text{C}$ . For each model run, Eq. 4 is fit through the point  
 291 cloud of  $R_e$  versus  $P_e$  to estimate  $S$  and a standard deviation associated with the curve  
 292 fit (Figure 1b). The  $CN$  is derived from the  $S$  estimate from the curve-fitting and the  
 293 standard deviation is scaled accordingly to yield a  $CN$  uncertainty estimate.

294 For each site, the  $CN$  is estimated using a linear interpolation of a look-up table  
 295 considering the impervious fraction within the eddy-covariance footprint (Cronshey et  
 296 al., 1985). Given soil texture influences  $CN$ , sand fraction (Brakensiek & Rawls, 1983;  
 297 Nachtergaele, 2001) obtained from a global data set (OpenLandMap, (Hengl, 2018)) is  
 298 used to constrain  $CN$  and provide uncertainty margins assuming an uncertainty of one-  
 299 third of the  $CN$  change in both directions from a one-level change in soil texture. If the  
 300 site  $CN$  uncertainty overlaps with the model  $CN$  uncertainty,  $I_{R,m}$  is assigned a value  
 301 of 1.

302 Indicator  $I_{R,t}$  addresses the rainfall- $R_s$  response times (Leopold, 1968). The lag  
 303 time is calculated as the difference between centroids of rainfall ( $P_{centroid}$ ) and  $R_s$  ( $R_{centroid}$ )  
 304 for the same events as the  $CN$  calculations (Figure 1a). Long-tail rainfall events are ex-  
 305 cluded when the  $R_{centroid}$  comes before the  $P_{centroid}$ . As eddy-covariance systems have  
 306 a footprint on the sub-square-kilometer scale (Feigenwinter et al., 2012), lag time is ex-  
 307 pected to be much faster than 30-60 minutes (Morin et al., 2001; Berne et al., 2004; Yao  
 308 et al., 2016), which is the model output resolution (Lipson et al., 2023a). Therefore, the  
 309 mean lag time needs to be less than one hour. The mean is preferred over the median  
 310 to also pinpoint models that occasionally have long lag times which would not affect the  
 311 median.

## 312 2.2 Models

313 The present study anonymously analyzes the water balance outputs from 19 Urban-  
 314 PLUMBER ULSMs (Table 2). Other Urban-PLUMBER ULSMs did not submit the nec-  
 315 essary outputs to allow for a water balance assessment. The outputs are for 20 sites cov-

316 ering a range of climates, impervious fractions, and observational periods (Table 3). As  
 317 two models did not run all sites, 377 runs are analyzed.

318 For each site, modelers were provided with the site characteristics and meteorolo-  
 319 gical forcing with 10-year spin-up data (Lipson et al., 2022a). The spin-up period re-  
 320 quired to reach equilibrium varies per model, with some requiring many years to come  
 321 to hydrological equilibrium with the forcing meteorology (Yang et al., 1995; Best & Grim-  
 322 mond, 2016). The 10 years of spin-up before the evaluation observations allowed the soil  
 323 moisture stores to equilibrate with local conditions prior to analysis. ERA5 reanalysis  
 324 data (Hersbach et al., 2020) are used to derive hourly forcing with bias-correction includ-  
 325 ing diurnal and seasonal effects for each site (Lipson et al., 2022a).

326 Depending on site data, evaluation is undertaken with 30- or 60-minute fluxes for  
 327 periods varying between 148 and 1827 days (average 912 days, Table 3). Similar to the  
 328 Urban-PLUMBER protocol, to minimize human errors, modelers received a preliminary  
 329 analysis of the water balance to help identify major issues and were encouraged to up-  
 330 date their results. This eliminated unit errors, added missing variables, and removed in-  
 331 active soil moisture layers.

332 For this study, we harmonize the hydrological model output. If a model only pro-  
 333 vided  $Q_E$  (unit:  $[W m^{-2}]$ ), it is converted to  $ET$  (unit:  $[mm d^{-1}]$ ) using latent heat  
 334 of vaporization accounting for air temperature (Bringfelt, 1986). When snow is present  
 335 the latent heat of fusion is added to the latent heat of vaporization to acquire the latent  
 336 heat of sublimation (Petrucci et al., 2010). In the forcing, precipitation is split into snow-  
 337 fall and rainfall. At only 30% of the sites, snowfall amounts to more than 10% of the pre-  
 338 cipitation. It is added as rainfall for one model without snow hydrology, while the two  
 339 others do not account for this input. Irrigation is simulated in two models. For all other  
 340 models, it is assumed to be zero.

### 341 3 Results

342 The 19 ULSMs show a wide spread in the average yearly water fluxes at all 20 sites  
 343 based on all 377 model runs (Figure 2). Overall, the model spread (whiskers, Figure 2)  
 344 is wider than the modeled ensemble mean flux (bars, Figure 2). Models show more vari-  
 345 ation in  $ET$  than in runoff. Sites with higher annual water input have more variability  
 346 in model output fluxes, for example, the relatively high fluxes in KR-Jungnang and SG-  
 347 TelokKurau compared to the lower yearly fluxes in PL-Lipowa and US-WestPhoenix.

#### 348 3.1 Water balance closure

349 Although the annual mean model ensemble almost closes the water balance at most  
 350 sites (Figure 2), most individual models do not close the water balance (Figure 3). Here,  
 351 closure is assumed when the sum of all fluxes (Eq. 3) is less than 3% of P+I. This oc-  
 352 curs in 57% of the model runs ( $I_A$ , Figure 4). In 25% of the model runs, non-closure ex-  
 353 ceeds 10% of P+I. Closure is model-related as the bias is similar across sites for each model  
 354 (Figure 3). Five models close the water balance in all runs, whereas four models account  
 355 for 48% of unclosed model runs. To assess the impact of model run length, the analy-  
 356 sis is repeated with sites with more than two years of observations yielding similar re-  
 357 sults.

#### 358 3.2 Evapotranspiration ( $ET$ )

359 Comparison of the modeled average diurnal range of the  $ET$  (Figure 5) shows the  
 360 highest inter-model spread at the peak of the daily cycle, with a range of 10-600% of the  
 361 model ensemble-mean flux. Along three sites with contrasting precipitation regimes (US-  
 362 WestPhoenix, AU-Preston, and SG-TelokKurau),  $ET$  increases as expected at wetter sites.

**Table 2.** Overview of the 19 urban land surface models in the water balance analysis based on Lipson et al. (2023a). Two models did not provide soil moisture output <sup>(1)</sup>. Three models capable of simulating irrigation did not include it in their Urban-PLUMBER runs <sup>(2)</sup>.

Model	Urban geometry	Vegetation	Soil hydrology	Snow accumulation	Irrigation	Reference
ASLUMv2.0	Canyon	Grass	Multi-layer	No	No <sup>2</sup>	Z.-H. Wang et al. (2013) C. Wang et al. (2021)
ASLUMv3.1	Canyon	Grass+trees	Multi-layer	No	No <sup>2</sup>	Z.-H. Wang et al. (2013) C. Wang et al. (2021)
CABLE	Non-urban	Separate tiles	Multi-layer	Veg.	No	Kowalczyk et al. (2006) Y. P. Wang et al. (2011)
CHTESSEL	Non-urban	Separate tiles	Multi-layer	Veg.	No	Balsamo et al. (2009) Boussetta et al. (2013)
CHTESSEL-U	Two-tile	Separate tiles	Multi-layer	Veg.+urban	No	McNorton et al. (2021) Balsamo et al. (2009)
CLMU5	Canyon	Grass+shrubs	Multi-layer	Urban	No	Oleson and Feddema (2020)
JULES 1T	One-tile	Separate tiles	Multi-layer	Veg.+urban	No	Best et al. (2011)
JULES 2T	Two-tile	Separate tiles	Multi-layer	Veg.+urban	No	Best et al. (2011)
JULES MOR	Two-tile	Separate tiles	Multi-layer	Veg.+urban	No	Best et al. (2011)
Lodz-SUEB	One-tile	Lumped with urban	Multi-layer <sup>1</sup>	Veg.+urban	No	Fortuniak (2003)
Manabe 1T	One-tile	Manabe bucket	One-layer	Veg.+urban	No	Best et al. (2011) Manabe (1969)
Manabe 2T	Two-tile	Manabe bucket	One-layer	Veg.+urban	No	Best et al. (2011) Manabe (1969)
NOAH-SLAB	One-tile	Separate tiles	Multi-layer	Veg.+urban	No	Kusaka et al. (2001) Ek et al. (2003)
NOAH-SLUCM	Canyon	Separate tiles	Multi-layer	Veg.+urban	No	Kusaka et al. (2001) Ek et al. (2003)
SNUUCM	Canyon	Separate tiles	Multi-layer <sup>1</sup>	Veg.	No	Ryu et al. (2011) Ek et al. (2003)
SUEWS	Two-tile	Separate tiles	One-layer	Veg.+urban	No <sup>2</sup>	Järvi et al. (2011) Ward et al. (2016)
TERRA 4.11	One-tile	Separate tiles	Multi-layer	Veg.	No	Wouters et al. (2015) Schulz and Vogel (2020)
UCLEM	Canyon	Grass+shrubs	One-layer	Veg.+urban	Yes	Thatcher and Hurley (2012)
UT&C	Canyon	Grass+shrubs+trees	Multi-layer	No	Yes	Lipson et al. (2018) Meili et al. (2020)

**Table 3.** Model (Table 2) outputs are analyzed for 20 sites (Lipson et al., 2022a). Only urban wind directions are included for the Minneapolis site. Characteristics include the local climate zone (LCZ, Stewart and Oke (2012), where 2 is compact mid-rise, 3 compact low-rise, 5 open mid-rise, and 6 open low-rise), impervious surface fraction ( $F_{imp}$ ), displacement height ( $z_d$ ), and eddy-covariance sensor height above ground level ( $z_s$ ).

Country	City (site)	Name	Lat. (°)	Lon. (°)	Observed period (days)	Köppen-Geiger climate	LCZ	$F_{imp}$	$z_d$ (m)	$z_s$ (m)	Reference	
Australia	Melbourne	(Preston)	AU-Preston	-37.73	145.01	475	Cfb	6	0.62	8	40	Coutts et al. (2007a)
Australia	Melbourne	(Surrey Hills)	AU-SurreyHills	-37.83	145.10	148	Cfb	6	0.54	8	38	Coutts et al. (2007b)
Canada	Vancouver	(Sunset)	CA-Sunset	49.23	-123.08	1827	Csb	6	0.68	3	25	Coutts et al. (2007a)
Finland	Helsinki	(Kumpula)	FI-Kumpula	60.20	24.96	1096	Dfb	mix	0.46	6	31	Coutts et al. (2007b)
Finland	Helsinki	(Torni)	FI-Torni	60.17	24.94	1096	Dfb	2	0.77	15	60	Christen et al. (2011)
France	Toulouse	(Capitole)	FR-Capitole	43.60	1.45	375	Cfa	2	0.90	11	48	Crawford and Christen (2015)
Greece	Heraklion		GR-HECKOR	35.34	25.13	367	Csa	3	0.92	17	27	Karsisto et al. (2016)
Japan	Tokyo	(Yoyogi)	JP-Yoyogi	35.66	139.68	1461	Cfa	2	0.92	28	52	Nordbo et al. (2013)
South Korea	Seoul	(Jungnang)	KR-Jungnang	37.59	127.08	825	Dwa	3	0.97	15	42	Järvi et al. (2018)
South Korea	Cheongju	(Ochang)	KR-Ochang	36.72	127.43	780	Dwa	5	0.47	4	19	Masson et al. (2008)
Mexico	Mexico City	(Escandon)	MX-Escandon	19.40	-99.18	470	Cwb	2	0.94	8	37	Goret et al. (2019)
Netherlands	Amsterdam		NL-Amsterdam	52.37	4.89	652	Cfb	2	0.68	10	40	Stagakis et al. (2019)
Poland	Lódź	(Lipowa)	PL-Lipowa	51.76	19.45	1827	Dfb	2	0.76	7	37	Hirano et al. (2015)
Poland	Lódź	(Narutowicza)	PL-Narutowicza	51.77	19.48	1827	Dfb	2	0.65	11	42	Ishidoya et al. (2020)
Singapore	Singapore	(Telok Kurau)	SG-TelokKurau	1.31	103.91	366	Af	3	0.85	7	24	J.-W. Hong et al. (2020)
UK	London	(King's college)	UK-KingsCollege	51.51	-0.12	638	Cfb	2	0.79	15	50	S.-O. Hong et al. (2023)
UK	Swindon		UK-Swindon	51.58	-1.80	715	Cfb	6	0.49	4	13	J.-W. Hong et al. (2019)
USA	Baltimore	(Cub hill)	US-Baltimore	39.41	-76.52	1826	Cfa	6	0.31	4	37	J.-W. Hong et al. (2020)
USA	Minneapolis		US-Minneapolis1	45.00	-93.19	1093	Dfa	6	0.21	3	40	Velasco et al. (2011)
USA	Phoenix	(West)	US-WestPhoenix	33.48	-112.14	382	Bwh	6	0.48	3	22	Velasco et al. (2011)
												Chow et al. (2014)
												Chow (2017)

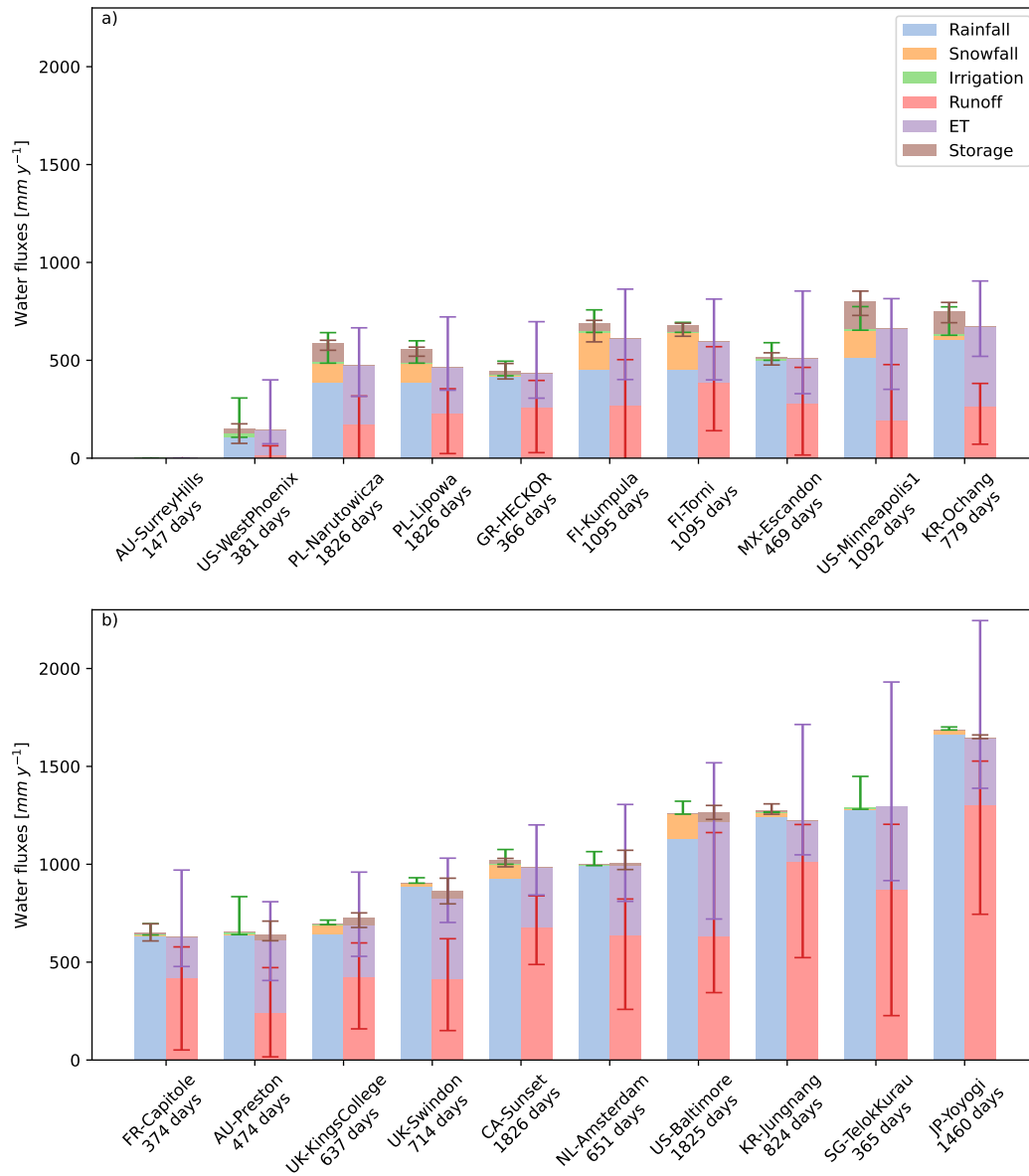


**Figure 2.** Ensemble mean (bars) and full range (minimum to maximum, whiskers) of the modeled annual water fluxes for all 20 sites ordered by increasing average annual precipitations. Modeled storage flux (Eq. 2, brown) appears on the left if a net input and right if a net loss. Values are means of all complete years in a data set (e.g. NL-Amsterdam: 2018-05-01 19:00 - 2019-05-01 19:00, 2018-05-01 20:00 - 2019-05-01 20:00, etc.). AU-SurreyHills has less than a year of observations.

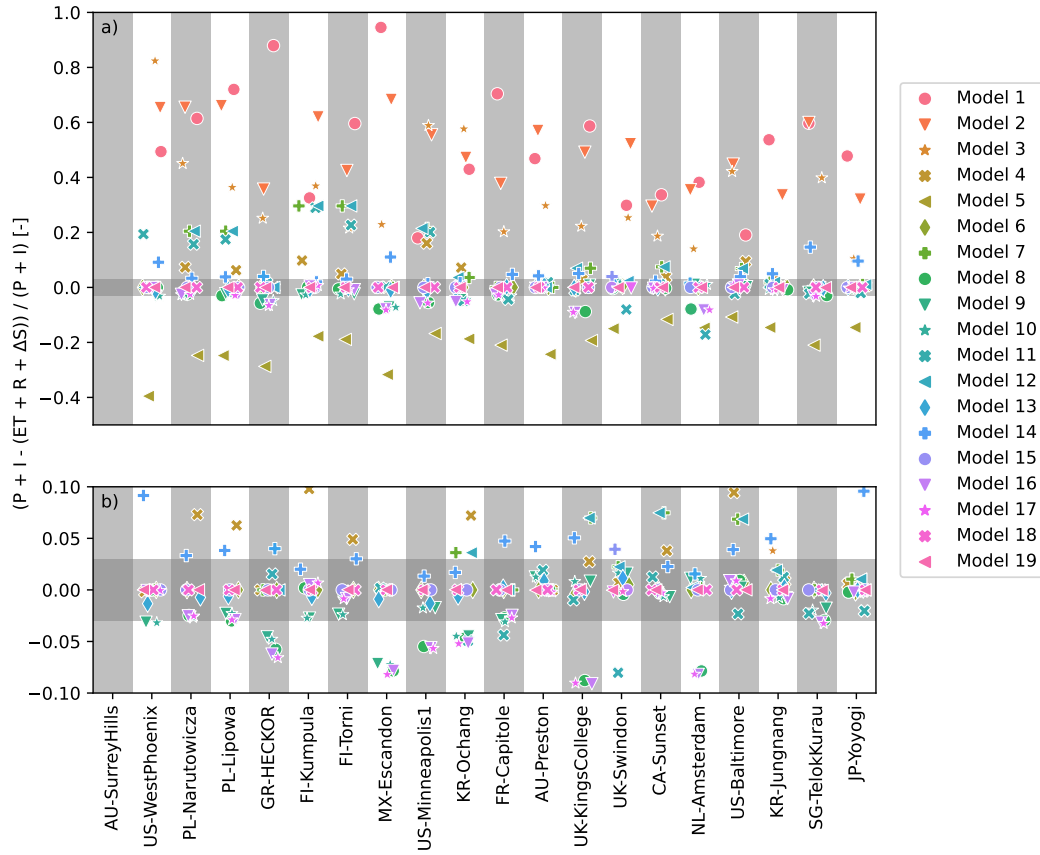


**Figure 3.** Annual water balance closure (Eq. 3) per model (marker) at 20 sites (by increasing average annual precipitation). Models with indicator  $I_A = 1$  (Table 1, horizontal shading) are shown in more detail in the lower panel (b).

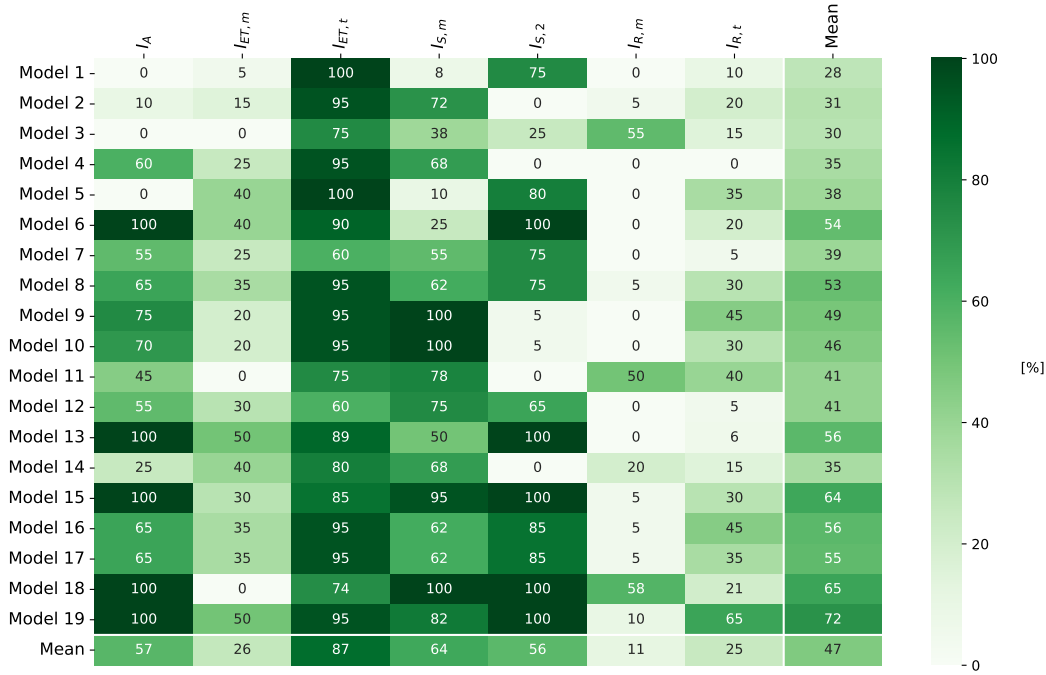


**Figure 4.** Overview of the indicators of the urban water balance representation (UWBR) score and constituent indicators (Table 1) over all sites. Means are corrected for missing model runs.

363 At US-WestPhoenix, all models but one underestimate  $ET$ . This underestimation likely  
 364 results from the absence of irrigation in nearly all models, while irrigation is common  
 365 at US-WestPhoenix (Templeton et al., 2018). At the other two sites, around half the mod-  
 366 els underestimate  $ET$  (Figure 5). Although for these sites the model medians are bet-  
 367 ter, the difficulty of capturing the correct flux magnitude is evident, as  $I_{ET,m}$  is passed  
 368 by only 26% of the model runs (Figure 4). No model passes this indicator at more than  
 369 half of the sites.

370 After different rainfall events, daily  $ET$  decreases with varying timescales in both  
 371 the observations and the models (Figure 6). The variation is higher amongst the mod-  
 372 eled than the observed drydowns. In contrast with the  $ET$  magnitude, the recession timescale  
 373 shows no link with the precipitation regime.  $I_{ET,t}$  shows the  $ET$  recession timescale is  
 374 captured correctly in 87% of the cases (Figure 4).

### 375 3.3 Water storage

376 Not all models have water storage values (Eq. 2) that are equal to the cumulative  
 377 net water flux (Eq. 1, Figure 7), which is seen across all sites (not shown). However, the  
 378 water storage should reflect the cumulative net water flux, as the storage change is equal  
 379 to the net water flux. For five models, the storage change is equal to the net water flux  
 380 at all sites. Minor differences occur in six models and large differences in six others. Two  
 381 models have no differences at sites without snowfall (e.g. AU-Preston) but large differ-  
 382 ences at sites with snowfall (e.g. CA-Sunset), as these models do not account for the snow-  
 383 fall in the input we see an increasing difference between the cumulative net water flux  
 384 and the water storage. The models with larger differences follow a seasonal cycle likely  
 385 caused by a non-restricted cumulative net water flux combined with restricted water stor-  
 386 age by soil storage capacity.

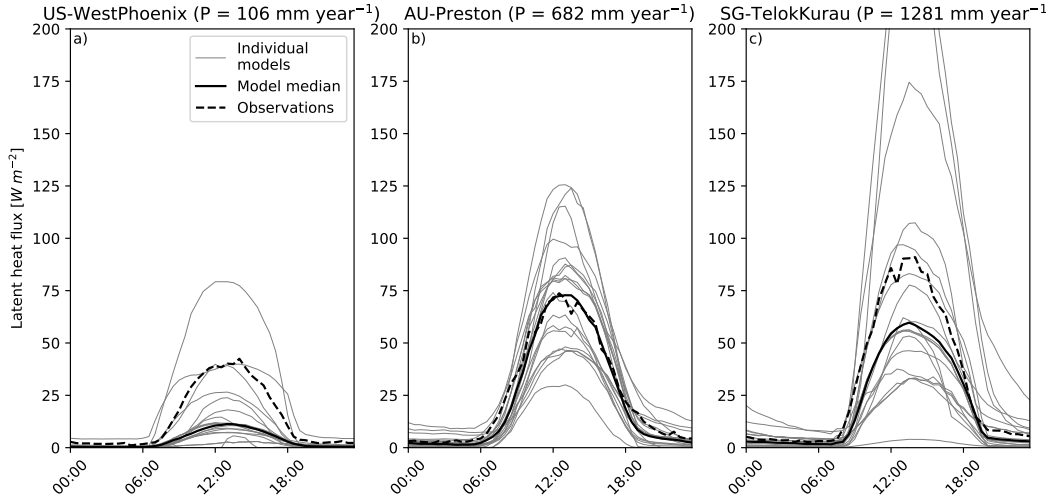


**Figure 5.** Illustration of modeled and observed (dashed) mean diurnal cycle of  $ET$  at three sites with contrasting annual rainfall: (a) US-WestPhoenix, (b) AU-Preston, and (c) SG-TelokKurau. Note that the observations are direct latent heat flux observations from eddy-covariance systems and do not refer to  $ET_{bench}$ .

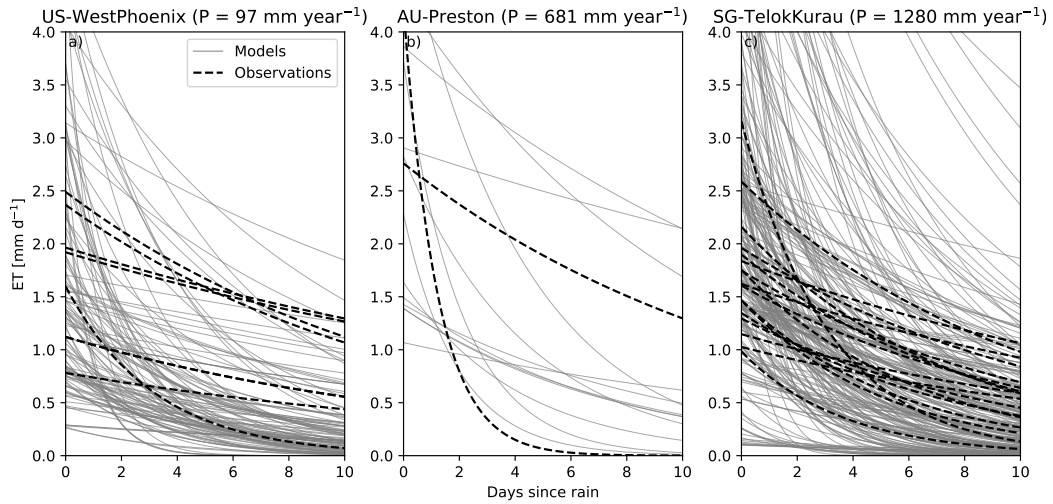


**Figure 6.** As Figure 5, but modeled (grey) and observed (black) daily  $ET$  following separate, individual rainfall events. Drydown events are selected based on their duration and data availability (see Jongen et al., 2022). Note that the observations are direct latent heat flux observations from eddy-covariance systems and do not refer to  $ET_{bench}$ .

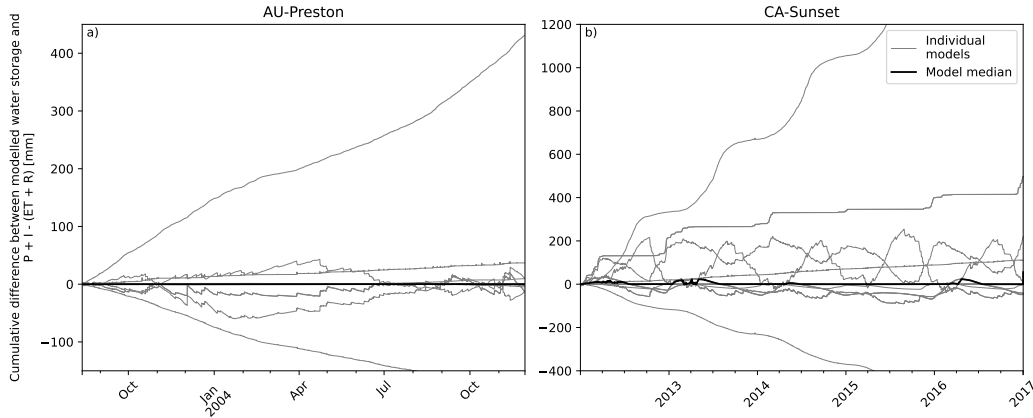


**Figure 7.** Cumulative difference between the water storage (Eq. 2) and cumulative net water flux (Eq. 1) at two representative sites for the entire model period for all models. Snowfall occurs at CA-Sunset, but not at AU-Preston. Some models are not visible as they are close to zero.

387 The range of modeled water storage exceeds the estimated site water storage capacity  
 388 ( $I_{S,m}$ ) in 64% of cases (Figure 4). Models 1 and 5 have the lowest score for this  
 389 indicator, because they have an inconsistency between the inputs and outputs (Eq. 3)  
 390 causing non-closure of the water balance at nearly all sites. Three models never exceed  
 391 the estimated water storage capacity.

392 How water storage relates to cumulative net water flux is linked to the individual  
 393 models given the consistent results across sites (Figure 9). With magnitude represented  
 394 by water balance closure, we focus on the timing by assessing the water storage relative  
 395 to the cumulative net water flux (Figure 8a-c). Model runs can have comparable direc-  
 396 tions but different patterns, e.g. model 11 (Figure 8a), comparable patterns but differ-  
 397 ent magnitudes of change, e.g. model 9 (Figure 8b), or virtually no differences (e.g. model  
 398 18, Figure 8c). The water storage change and the net water flux (Figure 8d-f) empha-  
 399 sizes the differences in timing, which is why the indicator uses the  $R^2$  of these deriva-  
 400 tives. Only five models have virtually no differences and thus an  $R^2$  of 1 (Figure 4). Over  
 401 half of the models have  $R^2$  greater than 0.9 indicating timing consistency ( $I_{S,t}$ , Figure  
 402 4).

### 403 3.4 Surface runoff ( $R_s$ )

404 All models have surface runoff triggered by precipitation, but the precipitation event  
 405 size causing  $R_s$  events differs between models (Figure 10). The model rather than the  
 406 site seems to explain triggering event size despite the variation amongst sites in imper-  
 407 vious fractions and precipitation regimes. This suggests that surface runoff parameter-  
 408 ization may be critical. Thus, we find a large inter-model spread in the cumulative mod-  
 409 eled  $R_s$  (Figure 2). One model is excluded as it does not output  $R_s$  separately from  $R_{sub}$ .  
 410 Ten models show the expected increase of cumulative  $R_s$  with increasing site impervi-  
 411 ous fraction ( $p > 0.05$ , Wald test (Wald, 1943)), whereas nine models do not (Figure S2).

412 Only in 43 of the 337 model runs, the  $CN$  (curve number: Section 2.1.4) is cap-  
 413 tured correctly, passing  $I_{R,m}$  (Figure 4), so all other model runs have no overlap with  
 414 the site estimates (see Section 2.1.4). Three models capture the  $CN$  correctly for at least  
 415 half of their model runs and are responsible for 32 of the successful model runs. Most  
 416 models do not match event precipitation and  $R_s$  relation. Most models underestimate  
 417 the  $CN$  relative to the site estimate (Figure S3). Underestimating the  $CN$  indicates a

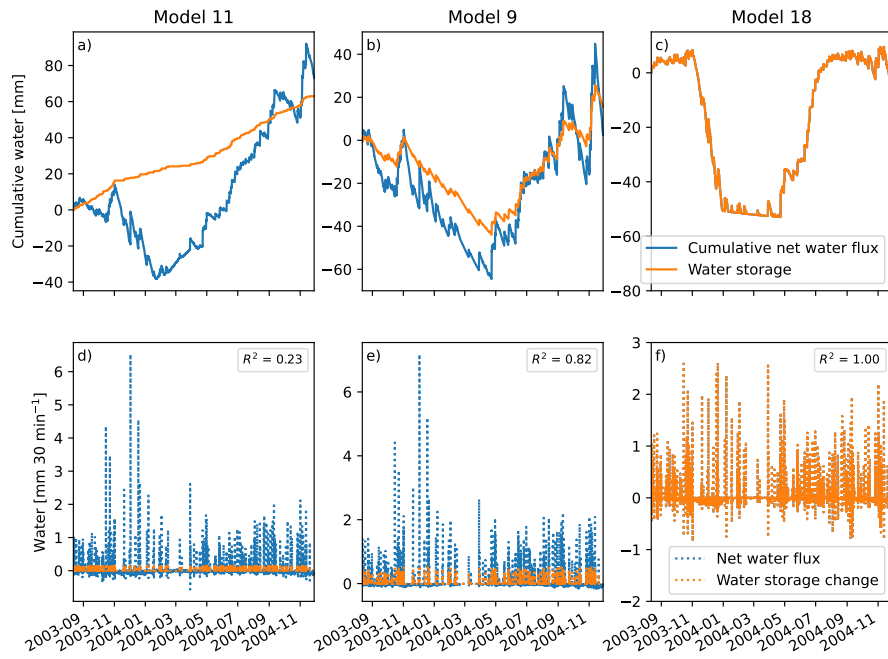


**Figure 8.** Illustration of the hourly water storage (Eq. 2) and the cumulative net water flux (Eq. 1) for 475 days at AU-Preston (a-c) and the water storage change and the net water flux (d-f) for three models with increasing coefficient of determination ( $R^2$ ) of the water storage change and the net water flux determined at (half-)hourly resolution.

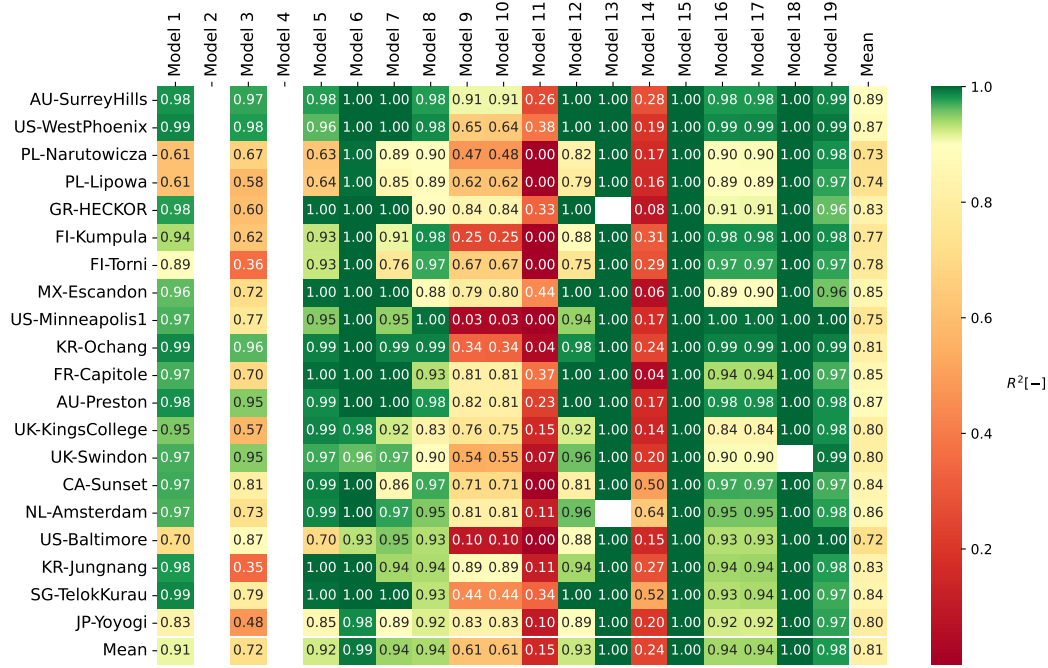


**Figure 9.** Coefficient of determination ( $R^2$ ) between (half-)hourly water storage change (Eq. 2) and net water flux (Eq. 1) by model and site. Green indicates the 0.9  $I_{S,t}$  threshold (Table 1). Missing results are shown as white (i.e. cannot calculate water storage change or net water flux). Figure 8 may aid interpretation of  $R^2$  values.

418 model is overestimating surface interception and/or soil infiltration, reducing  $R_s$  (Equation 4).  
 419

420 One in four model runs accurately captures the fast  $R_s$  response in the lag time  
 421 (Figure 4) with  $I_{R,t}$  passed by 25% of the model runs. With very short lag times expected,  
 422 only overestimates are simulated. Most lag times averaged per model run are less than  
 423 five hours, but exceptionally they are over 100 hours. Average lag times per model run  
 424 are shown in Figure S4.

### 425 3.5 Urban water balance representation (UWBR) score

426 Across all model runs, the mean UWBR score amounts to 3.3 out of the possible  
 427 7 (Figure 4). Although the overall pass rate across all indicators and models is 47%, pass  
 428 rates strongly vary per indicator. Notably, 87% passes  $I_{ET,t}$ , while only 11% passes  $I_{R,m}$ .  
 429 Pass rates also differ among models from 28% to 72%. Only one model run passes all  
 430 indicators, while 10 model runs have a score of 6 out of 7. Model 19 accounts for five of  
 431 these eleven high-scoring runs. If a model closes the water balance ( $I_A$ ), it generally scores  
 432 better on both storage indicators. In contrast, models with a high passing percentage  
 433 for one  $ET$  indicator do not systematically score better for the other  $ET$  indicator. Over-  
 434 all, the  $ET$  timing ( $I_{ET,t}$ ) is captured better than its cumulative magnitude ( $I_{ET,m}$ ). A  
 435 similar pattern is seen in the  $R_s$  indicators with the timing ( $I_{R,t}$ ) captured slightly bet-  
 436 ter than magnitude ( $I_{R,m}$ ).

437 Generally, pass rates per indicator show a dependence on the model (Figure 4). This  
 438 dependence is not found for sites (Figure S5). There is no relation evident between UWBR  
 439 score and model approach (e.g. built surface, soil hydrology, Table 2), but the model is

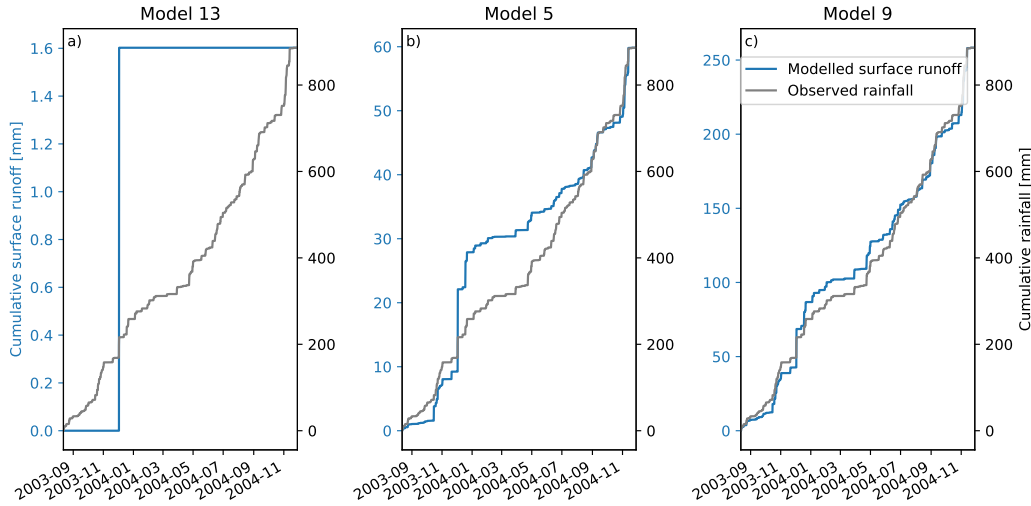


**Figure 10.** Illustration of surface runoff triggered for different AU-Preston precipitation events by three models (a) 13, (b) 5, and (c) 9. Note, the left-hand Y axis (surface runoff) increases (a→c), whereas the right-hand side Y axis (precipitation) is the same for all.

440 more influential than the site on UWBR score. As the Lipson et al. (2023a) classifica-  
 441 tion (Table 2) was not developed with the water balance representation as its original  
 442 goal, further work would be needed to identify what model attributes are key to better  
 443 UWBR score.

### 444 3.6 Linking the water and energy balance

445 Surprisingly, models do not appear to capture any aspect of the latent heat flux  
 446 more accurately if their UWBR score is higher. The UWBR score does not significantly  
 447 correlate with better ranking on any of the four metrics evaluating the (half-)hourly modeled  
 448  $Q_E$ : the  $R^2$ ,  $\sigma_{norm}$ ,  $RMSE_s$ , and  $RMSE_u$  ( $p > 0.05$ , Wald test, Figure S6). These  
 449 correlations remain absent if one of the indicators is omitted from the analysis. The lack  
 450 of correlation may be the result of the low number (11) of runs with a UWBR score higher  
 451 than 5 (Figure 4) effectively reducing the UWBR score range. Given the lack of relations  
 452 between the UWBR score and  $Q_E$  metrics, the  $Q_E$  is not better captured in model runs  
 453 that pass more indicators of a realistic water balance representation, thus refuting our  
 454 hypothesis that the urban water balance skill positively impacts simulated energy fluxes.

## 455 4 Discussion and conclusions

456 This study assesses the water balance representation in 19 ULSMs from the Urban-  
 457 PLUMBER project. It appears the water balance is not closed (within 3%) in 57% of  
 458 the model-site runs. The considerable spread in water fluxes is as wide as the absolute  
 459 flux magnitude at all sites. For both  $ET$  and  $R_s$ , the timing is captured better than the  
 460 flux magnitude. Modeled water storage dynamics (Eq. 2) are inconsistent with the net  
 461 water flux (Eq. 1) in 44% of the models. Refuting our hypothesis, a better water bal-  
 462 ance representation does not result in more accurate latent heat fluxes. However, it is  
 463 clear that the urban water balance is imperfectly incorporated into ULSMs and more  
 464 proper physically-based representations are required.

465 Five models close the water balance at all sites (Models 6, 13, 15, 18, and 19), while  
 466 three never reach closure (Models 1, 3, and 5). The other models close the water bal-  
 467 ance at some sites. For several non-closing models, we identify the causes. One model  
 468 implicitly assumes an infinite source or sink of soil moisture by adapting the modeled  
 469 soil moisture when it exceeds hard-coded limits adding or removing water to remain within  
 470 these limits (Model 11). Two other models do not fully couple all processes, such as runoff  
 471 and evaporation calculations occurring without water availability feedback between pro-  
 472 cesses (Models 1 and 5). Such uncoupled processes may also explain inconsistent water  
 473 storage dynamics and net water flux. Three models have groundwater flux, which is not  
 474 included in the model output (Models 8, 16, and 17). One model without a snow mod-  
 475 ule disregarded all snowfall creating a mismatch between real and modeled input (Model  
 476 2). For one model, we suspect a very shallow soil layer causes large numerical errors re-  
 477 sulting in an unclosed water balance (Model 4). Fortunately, model improvements should  
 478 be able to eliminate these issues for most models.

479 Evidence is found that the models would benefit from reevaluating their runoff par-  
 480 ameterizations. The runoff volumes are poorly captured, resulting in  $I_{R,m}$  having the  
 481 poorest overall pass rate (Figure 4). Runoff has not been evaluated in previous ULSM  
 482 comparisons and suffers here from a lack of direct observations and small areas being mod-  
 483 eled ( $<1 \text{ km}^2$ ). The lack of correlation between modeled cumulative  $R_s$  and the imper-  
 484 vious fraction is worrying given the well-documented relation (Shuster et al., 2005; Ja-  
 485 cobson, 2011). However, many models use relatively simple approaches, such as a con-  
 486 stant fraction of rainfall that runs off independent of site characteristics, rainfall inten-  
 487 sity, or soil moisture state. Others use poorly constrained parameters, such as how much  
 488 water is routed between sub-grid tiles. Future work could help to constrain such para-  
 489 meters, while the simple approaches could be improved relatively straightforwardly.

490 Despite the lack of evidence showing a link between the UWBR score and  $Q_E$  per-  
 491 formance, the incomplete representation of the water balance may contribute to the poor  
 492 latent heat flux performance of the ULSMs. The design of the UWBR score may not be  
 493 successful in revealing an existing link between the UWBR score and  $Q_E$  performance,  
 494 as the UWBR score indicators assess the water balance based on physical realism and  
 495 expectations derived from the literature. While a higher UWBR score indicates a more  
 496 physically consistent water balance, it may still be an incorrect simulation. The oppo-  
 497 site is also true, as, without physical constraints, machine learning approaches show good  
 498 results for  $Q_E$  (Vulova et al., 2021). Apart from that, a potential link between the wa-  
 499 ter balance representation and the  $Q_E$  performance may be hidden by other elements  
 500 affecting  $Q_E$  performance. These elements could be other components of the model (e.g.  
 501 the energy balance representation) or human errors. Yet, we do find a poor performance  
 502 for  $Q_E$  consistent with the literature showing  $Q_E$  is among the most challenging fluxes  
 503 to model (Grimmond et al., 2011; Lipson et al., 2023a). As the energy and water bal-  
 504 ance are directly connected, we hypothesize potential errors in the water balance are caus-  
 505 ing, and not being caused by, the poor performance of  $Q_E$ , as the short runoff timescales  
 506 in urban areas on a neighborhood scale dictate the water availability for  $Q_E$  and not the  
 507 other way around. Hence, good model performance for the latent and sensible heat flux  
 508 cannot be achieved without properly representing both balances. Thus, we believe an  
 509 improved representation of the water balance will assist in latent heat flux simulation  
 510 and other energy fluxes.

511 This first systematic analysis of urban water balance modeling is an opportunis-  
 512 tic study taking advantage of model outputs, model characterizations, and observations  
 513 gathered for the Urban PLUMBER project (Lipson et al., 2023a, 2022a). The Urban-  
 514 PLUMBER setup affects this study via (1) the diversity of model outputs linked to their  
 515 range of modeling approaches, and (2) a lack of observations for all the water balance  
 516 terms. Intentionally, a wide range of modeling approaches are analyzed with both de-  
 517 fault parameters and provided parameters implemented by modelers (Lipson et al., 2023a),

518 impacting the model results and performance. For example, numerical discretization of  
 519 soil layers can cause a flawed, reduced moisture drydown linked to irregular soil layer depths  
 520 that enhance evaporation (MacKay et al., 2022). Ongoing land surface model develop-  
 521 ments to capture and link more processes increase both their scope and complexity, but  
 522 the number of differing aspects complicates a systematic analysis aiming to attribute per-  
 523 formance to certain aspects (Fisher & Koven, 2020; Blyth et al., 2021). To minimize hu-  
 524 man error, Urban-PLUMBER allowed resubmission of model outputs after web-based  
 525 and manual checks. As these checks did not address the water balance, we provided an  
 526 additional basic analysis of the water balance results to catch other human errors with  
 527 encouragement to resubmit updated outputs. Unfortunately, resubmission reduces but  
 528 does not eliminate human errors. All differences other than the water balance represen-  
 529 tation hinder the attribution of the model performance to the water balance concept as  
 530 they explain the large variety in model performance amongst models that capture the  
 531 water balance equally accurately. Ideally, these differences would be eliminated by de-  
 532 veloping a multi-model framework in the future (Sadegh et al., 2019) and characteriz-  
 533 ing model types based on water balance approaches. Such a characterization could al-  
 534 low for teasing out more detailed strengths and weaknesses of water balance represen-  
 535 tations.

536 Lack of observations (e.g. runoff, soil moisture) prevents direct assessment for many  
 537 water balance terms. Hence, we develop a new alternative using quantitative indicators.  
 538 Each indicator addresses a water balance process and checks whether it complies with  
 539 physical limits, the model itself, or previous research. We refrain from weighting the in-  
 540 dicators to minimize the score subjectivity and prevent one indicator from controlling  
 541 the outcome. The systematic removal of one of the seven indicators allows us to confirm  
 542 the UWBR score is not driven by one indicator.

543 Here, we show ULSMs produce a wide range of water balance results but often do  
 544 not realistically represent important hydrological processes. Although our results are for  
 545 offline ULSMs, we expect the identified issues will persist in a coupled setting on any scale  
 546 (e.g., with mesoscale atmospheric models). ULSMs could be improved by ensuring they  
 547 close the water balance and updating runoff parameterizations. Ideally, future energy-  
 548 water-carbon studies will try to gather both a wider range of observations but also mod-  
 549 eled processes. This will aid improvement of model processes and their feedbacks. How-  
 550 ever, the complexity of the urban landscape (e.g. different definitions between eddy co-  
 551 variance footprints, and runoff catchments) will require nested model runs and obser-  
 552 vations to ensure consistency of all. We recommend routine assessment of water balance  
 553 closure in ULSM development phase applying the indicators of the UWBR score. In a  
 554 broader context, both model evaluations and comparisons should extend beyond the tar-  
 555 get variables of the model to all processes that directly influence these variables. This  
 556 will benefit the broader delivery of integrated urban services (WMO, 2019) and facili-  
 557 tate urban resilience across time scales.

## 58 5 Open research

559 All observation data from this study are openly available at Zenodo via <https://doi.org/10.5281/zenodo.6590>  
 560 (Lipson et al., 2022b). Model results and benchmarks (Lipson & Best, 2022) for AU-preston  
 561 are archived at Zenodo. Model results for the other sites are visualized at [https://urban-  
 562 plumber.github.io/sites](https://urban-plumber.github.io/sites) and will be published together with phase 2.

## 563 Acknowledgments

564 We acknowledge the Urban-PLUMBER project team and all observation and modeling  
 565 participants providing the data set for this research. We would like to thank Judith Boe-  
 566 kee, Andrew Frost, and Valentina Marchionni for the fruitful discussions. Harro Jongen  
 567 acknowledges this research was supported by the WIMEK PhD grant 2020. Mathew Lip-

568 son acknowledges support from the Australian Research Council (ARC) Centre of Ex-  
 569 cellence for Climate System Science (grant CE110001028), National Computational In-  
 570 frastructure (NCI) Australia and the Bureau of Meteorology, Australia. Gert-Jan Steen-  
 571 eveld acknowledges support from the Amsterdam Institute for Advanced Metropolitan  
 572 Solutions (AMS Institute, project VIR16002) and the Netherlands Organisation for Sci-  
 573 entific Research (NWO, Project 864.14.007). Sue Grimmond acknowledges support from  
 574 ERC Urbisphere (grant 855055). Matthias Demuzere was supported by the ENLIGHT  
 575 project, funded by the German Research Foundation (DFG) under grant no. 437467569.  
 576 Ting Sun is supported by UKRI NERC Independent Research Fellowship (NE/P018637/2).  
 577 Ruidong Li is supported by CSC scholarship. Keith Oleson’s contribution is based upon  
 578 work supported by the NSF National Center for Atmospheric Research, which is a ma-  
 579 jor facility sponsored by the U.S. National Science Foundation under Cooperative Agree-  
 580 ment No. 1852977. Chenghao Wang acknowledges support from the National Science  
 581 Foundation (NSF) under grant No. OIA-2327435 and the National Oceanic and Atmo-  
 582 spheric Administration (NOAA) under grant No. NA21OAR4590361.

## 583 References

- 584 Balsamo, G., Beljaars, A., Scipal, K., Viterbo, P., van den Hurk, B., Hirschi, M., &  
 585 Betts, A. K. (2009). A revised hydrology for the ECMWF model: Verification  
 586 from field site to terrestrial water storage and impact in the integrated forecast  
 587 system. *Journal of Hydrometeorology*, *10*(3), 623–643.
- 588 Berne, A., Delrieu, G., Creutin, J.-D., & Obled, C. (2004). Temporal and spatial  
 589 resolution of rainfall measurements required for urban hydrology. *Journal of*  
 590 *Hydrology*, *299*(3-4), 166–179.
- 591 Berthier, E., Andrieu, H., & Rodriguez, F. (1999). The Rezé urban catchments  
 592 database. *Water Resources Research*, *35*(6), 1915–1919.
- 593 Best, M. J., Abramowitz, G., Johnson, H., Pitman, A., Balsamo, G., Boone, A., ...  
 594 others (2015). The plumbing of land surface models: benchmarking model  
 595 performance. *Journal of Hydrometeorology*, *16*(3), 1425–1442.
- 596 Best, M. J., & Grimmond, C. S. B. (2016). Modeling the partitioning of turbulent  
 597 fluxes at urban sites with varying vegetation cover. *Journal of Hydrometeorol-*  
 598 *ogy*, *17*(10), 2537–2553.
- 599 Best, M. J., Pryor, M., Clark, D., Rooney, G., Essery, R., Ménard, C., ... oth-  
 600 ers (2011). The Joint UK Land Environment Simulator (JULES), model  
 601 description—part 1: energy and water fluxes. *Geoscientific Model Development*,  
 602 *4*(3), 677–699.
- 603 Bjorkegren, A., Grimmond, C. S. B., Kotthaus, S., & Malamud, B. (2015). CO<sub>2</sub>  
 604 emission estimation in the urban environment: Measurement of the CO<sub>2</sub> stor-  
 605 age term. *Atmospheric Environment*, *122*, 775–790.
- 606 Blyth, E. M., Arora, V. K., Clark, D. B., Dadson, S. J., De Kauwe, M. G.,  
 607 Lawrence, D. M., ... others (2021). Advances in land surface modelling.  
 608 *Current Climate Change Reports*, *7*(2), 45–71.
- 609 Botzen, W., Martinius, M., Bröde, P., Folkerts, M., Ignjacevic, P., Estrada, F., ...  
 610 Daanen, H. (2020). Economic valuation of climate change-induced mortality:  
 611 age dependent cold and heat mortality in the Netherlands. *Climatic Change*,  
 612 *162*(2), 545–562.
- 613 Boussetta, S., Balsamo, G., Beljaars, A., Panareda, A.-A., Calvet, J.-C., Jacobs, C.,  
 614 ... others (2013). Natural land carbon dioxide exchanges in the ECMWF  
 615 integrated forecasting system: Implementation and offline validation. *Journal*  
 616 *of Geophysical Research: Atmospheres*, *118*(12), 5923–5946.
- 617 Brakensiek, D. L., & Rawls, W. J. (1983). Green-Ampt infiltration model para-  
 618 meters for hydrologic classification of soils. In *Advances in irrigation and*  
 619 *drainage: surviving external pressures* (pp. 226–233).
- 620 Bringfelt, B. (1986). *Test of a forest evapotranspiration model*. SMHI.

- 621 Carlyle-Moses, D. E., Livesley, S., Baptista, M. D., Thom, J., & Szota, C. (2020).  
 622 Urban trees as green infrastructure for stormwater mitigation and use. *Forest-*  
 623 *Water Interactions*, 397–432.
- 624 Chakravarti, I., Laha, R., & Roy, J. (1967). *Handbook of methods of applied statis-*  
 625 *tics. volume i: Techniques of computation, descriptive methods, and statistical*  
 626 *inference*. John Wiley & Sons, Incorporated.
- 627 Châtelet, E. (1740). *Institutions de physique*. Paris.
- 628 Chow, W. T. (2017). *Eddy covariance data measured at the CAP LTER flux tower*  
 629 *located in the west Phoenix, AZ neighborhood of Maryvale from 2011-12-16*  
 630 *through 2012-12-31*. Environmental Data Initiative.
- 631 Chow, W. T., Volo, T. J., Vivoni, E. R., Jenerette, G. D., & Ruddell, B. L. (2014).  
 632 Seasonal dynamics of a suburban energy balance in Phoenix, Arizona. *Internat-*  
 633 *ional Journal of Climatology*, 34(15), 3863–3880.
- 634 Christen, A., Coops, N., Crawford, B., Kellett, R., Liss, K., Olchovski, I., ... Voogt,  
 635 J. (2011). Validation of modeled carbon-dioxide emissions from an urban  
 636 neighborhood with direct eddy-covariance measurements. *Atmospheric Envi-*  
 637 *ronment*, 45(33), 6057–6069.
- 638 Coutts, A. M., Beringer, J., & Tapper, N. J. (2007a). Characteristics influencing the  
 639 variability of urban CO<sub>2</sub> fluxes in Melbourne, Australia. *Atmospheric Environ-*  
 640 *ment*, 41(1), 51–62.
- 641 Coutts, A. M., Beringer, J., & Tapper, N. J. (2007b). Impact of increasing urban  
 642 density on local climate: Spatial and temporal variations in the surface en-  
 643 ergy balance in Melbourne, Australia. *Journal of Applied Meteorology and*  
 644 *Climatology*, 46(4), 477–493.
- 645 Crawford, B., & Christen, A. (2015). Spatial source attribution of measured ur-  
 646 ban eddy covariance co<sub>2</sub> fluxes. *Theoretical and Applied Climatology*, 119,  
 647 733–755.
- 648 Crawford, B., Grimmond, C., & Christen, A. (2011). Five years of carbon dioxide  
 649 fluxes measurements in a highly vegetated suburban area. *Atmospheric Envi-*  
 650 *ronment*, 45(4), 896–905.
- 651 Cronshey, R., Roberts, R., & Miller, N. (1985). Urban hydrology for small water-  
 652 sheds (tr-55 rev.). In *Hydraulics and hydrology in the small computer age* (pp.  
 653 1268–1273).
- 654 Demuzere, M., Kittner, J., Martilli, A., Mills, G., Moede, C., Stewart, I. D., ...  
 655 Bechtel, B. (2022). A global map of local climate zones to support earth sys-  
 656 tem modelling and urban scale environmental science. *Earth System Science*  
 657 *Data Discussions*, 2022, 1–57.
- 658 Ek, M., Mitchell, K., Lin, Y., Rogers, E., Grunmann, P., Koren, V., ... Tarpley, J.  
 659 (2003). Implementation of noah land surface model advances in the national  
 660 centers for environmental prediction operational mesoscale eta model. *Journal*  
 661 *of Geophysical Research: Atmospheres*, 108(D22).
- 662 Feigenwinter, C., Vogt, R., & Christen, A. (2012). Eddy covariance measurements  
 663 over urban areas. *Eddy covariance: A practical guide to measurement and data*  
 664 *analysis*, 377–397.
- 665 Fisher, R. A., & Koven, C. D. (2020). Perspectives on the future of land surface  
 666 models and the challenges of representing complex terrestrial systems. *Journal*  
 667 *of Advances in Modeling Earth Systems*, 12(4), e2018MS001453.
- 668 Fletcher, T. D., Andrieu, H., & Hamel, P. (2013). Understanding, management  
 669 and modelling of urban hydrology and its consequences for receiving waters: A  
 670 state of the art. *Advances in water resources*, 51, 261–279.
- 671 Foken, T., Leuning, R., Oncley, S. R., Mauder, M., & Aubinet, M. (2012). Corre-  
 672 ctions and data quality control. In *Eddy covariance* (pp. 85–131). Springer.
- 673 Fortuniak, K. (2003). A slab surface energy balance model (SUEB) and its appli-  
 674 cation to the study on the role of roughness length in forming an urban heat  
 675 island. *Acta Universitatis Wratislaviensis*, 2542, 368–377.

- 676 Fortuniak, K., Kłysik, K., & Siedlecki, M. (2006). New measurements of the en-  
677 ergy balance components in Łódź. In *Preprints, sixth international conference*  
678 *on urban climate, Göteborg, Sweden* (pp. 12–16).
- 679 Fortuniak, K., Pawlak, W., & Siedlecki, M. (2013). Integral turbulence statistics  
680 over a central European city centre. *Boundary-Layer Meteorology*, *146*, 257–  
681 276.
- 682 Franssen, H. H., Stöckli, R., Lehner, I., Rotenberg, E., & Seneviratne, S. I. (2010).  
683 Energy balance closure of eddy-covariance data: A multisite analysis for Eu-  
684 ropean FLUXNET stations. *Agricultural and Forest Meteorology*, *150*(12),  
685 1553–1567.
- 686 Gasparrini, A., Guo, Y., Sera, F., Vicedo-Cabrera, A. M., Huber, V., Tong, S., ...  
687 others (2017). Projections of temperature-related excess mortality under  
688 climate change scenarios. *The Lancet Planetary Health*, *1*(9), e360–e367.
- 689 Goret, M., Masson, V., Schoetter, R., & Moine, M.-P. (2019). Inclusion of CO<sub>2</sub>  
690 flux modelling in an urban canopy layer model and an evaluation over an old  
691 European city centre. *Atmospheric Environment: X*, *3*, 100042.
- 692 Grimmond, C. S. B. (2006). Progress in measuring and observing the urban atmo-  
693 sphere. *Theoretical and Applied Climatology*, *84*(1), 3–22.
- 694 Grimmond, C. S. B., Best, M. J., Barlow, J., Arnfield, A., Baik, J.-J., Baklanov, A.,  
695 ... others (2009). Urban surface energy balance models: model characteristics  
696 and methodology for a comparison study. In *Meteorological and air quality*  
697 *models for urban areas* (pp. 97–123). Springer.
- 698 Grimmond, C. S. B., Blackett, M., Best, M. J., Baik, J.-J., Belcher, S., Beringer, J.,  
699 ... others (2011). Initial results from phase 2 of the international urban en-  
700 ergy balance model comparison. *International Journal of Climatology*, *31*(2),  
701 244–272.
- 702 Grimmond, C. S. B., Blackett, M., Best, M. J., Barlow, J., Baik, J., Belcher, S.,  
703 ... others (2010). The international urban energy balance models compar-  
704 ison project: first results from phase 1. *Journal of applied meteorology and*  
705 *climatology*, *49*(6), 1268–1292.
- 706 Grimmond, C. S. B., & Oke, T. R. (1986). Urban water balance: 2. results from  
707 a suburb of Vancouver, British Columbia. *Water Resources Research*, *22*(10),  
708 1404–1412.
- 709 Grimmond, C. S. B., & Oke, T. R. (1991). An evapotranspiration-interception  
710 model for urban areas. *Water Resources Research*, *27*(7), 1739–1755.
- 711 Grimmond, C. S. B., & Oke, T. R. (2002). Turbulent heat fluxes in urban areas:  
712 Observations and a local-scale urban meteorological parameterization scheme  
713 (lumps). *Journal of Applied Meteorology and Climatology*, *41*(7), 792–810.
- 714 Hamdi, R., Kusaka, H., Doan, Q.-V., Cai, P., He, H., Luo, G., ... others (2020).  
715 The state-of-the-art of urban climate change modeling and observations. *Earth*  
716 *Systems and Environment*, 1–16.
- 717 Hamdi, R., & Schayes, G. (2007). Validation of Martilli’s urban boundary layer  
718 scheme with measurements from two mid-latitude European cities. *Atmo-*  
719 *spheric Chemistry and Physics*, *7*(17), 4513–4526.
- 720 Heaviside, C., Vardoulakis, S., & Cai, X.-M. (2016). Attribution of mortality to the  
721 urban heat island during heatwaves in the West Midlands, UK. *Environmental*  
722 *health*, *15*(1), 49–59.
- 723 Hellsten, A., Luukkonen, S.-M., Steinfeld, G., Kanani-Sühring, F., Markkanen, T.,  
724 Järvi, L., ... Raasch, S. (2015). Footprint evaluation for flux and concentra-  
725 tion measurements for an urban-like canopy with coupled lagrangian stochastic  
726 and large-eddy simulation models. *Boundary-Layer Meteorology*, *157*(2),  
727 191–217.
- 728 Henderson-Sellers, A., McGuffie, K., & Pitman, A. (1996). The project for intercom-  
729 parison of land-surface parametrization schemes (PILPS): 1992 to 1995. *Cli-*  
730 *mate Dynamics*, *12*(12), 849–859.

- 731 Hengl, T. (2018). *Sand content in % (kg/kg) at 6 standard depths (0, 10, 30, 60,*  
732 *100 and 200 cm) at 250 m resolution (version v0. 2) [data set].* Zenodo. doi:  
733 <https://doi.org/10.5281/zenodo.2525662>
- 734 Hersbach, H., Bell, B., Berrisford, P., Hirahara, S., Horányi, A., Muñoz-Sabater, J.,  
735 ... others (2020). The ERA5 global reanalysis. *Quarterly Journal of the Royal*  
736 *Meteorological Society*, *146*(730), 1999–2049.
- 737 Hertwig, D., Grimmond, C. S. B., Hendry, M. A., Saunders, B., Wang, Z., Jeoffrion,  
738 M., ... others (2020). Urban signals in high-resolution weather and climate  
739 simulations: role of urban land-surface characterisation. *Theoretical and Ap-*  
740 *plied Climatology*, *142*(1), 701–728.
- 741 Hirano, T., Sugawara, H., Murayama, S., & Kondo, H. (2015). Diurnal variation of  
742 CO<sub>2</sub> flux in an urban area of Tokyo. *Sola*, *11*, 100–103.
- 743 Hirschi, M., Michel, D., Lehner, I., & Seneviratne, S. I. (2017). A site-level compari-  
744 son of lysimeter and eddy covariance flux measurements of evapotranspiration.  
745 *Hydrology and Earth System Sciences*, *21*(3), 1809–1825.
- 746 Hong, J.-W., Hong, J., Chun, J., Lee, Y. H., Chang, L.-S., Lee, J.-B., ... Joo, S.  
747 (2019). Comparative assessment of net CO<sub>2</sub> exchange across an urbanization  
748 gradient in Korea based on eddy covariance measurements. *Carbon Balance*  
749 *and Management*, *14*(1), 1–18.
- 750 Hong, J.-W., Lee, K., & Hong, J. (2020). *Observational data of Ochang and Jung-*  
751 *namg in Korea, EAPL at Yonsei University [data set].*
- 752 Hong, S.-O., Kim, J., Byun, Y.-H., Hong, J., Hong, J.-W., Lee, K., ... Kim, Y.-H.  
753 (2023). Intra-urban variations of the CO<sub>2</sub> fluxes at the surface-atmosphere  
754 interface in the Seoul Metropolitan Area. *Asia-Pacific Journal of Atmospheric*  
755 *Sciences*, 1–15.
- 756 Howard, L. (1833). *The climate of london deduced from meteorological observations*  
757 *made in the metropolis and various places around it.* (Vol. 1). W. Phillips.
- 758 Ishidoya, S., Sugawara, H., Terao, Y., Kaneyasu, N., Aoki, N., Tsuboi, K., & Kondo,  
759 H. (2020). O<sub>2</sub>: CO<sub>2</sub> exchange ratio for net turbulent flux observed in an urban  
760 area of Tokyo, Japan, and its application to an evaluation of anthropogenic  
761 CO<sub>2</sub> emissions. *Atmospheric Chemistry and Physics*, *20*(9), 5293–5308.
- 762 Jacobson, C. R. (2011). Identification and quantification of the hydrological impacts  
763 of imperviousness in urban catchments: A review. *Journal of Environmental*  
764 *Management*, *92*(6), 1438–1448.
- 765 Järvi, L., Grimmond, C. S. B., & Christen, A. (2011). The surface urban energy and  
766 water balance scheme (SUEWS): Evaluation in Los Angeles and Vancouver.  
767 *Journal of Hydrology*, *411*(3-4), 219–237.
- 768 Järvi, L., Rannik, Ü., Kokkonen, T. V., Kurppa, M., Karppinen, A., Kouznetsov,  
769 R. D., ... Wood, C. R. (2018). Uncertainty of eddy covariance flux measure-  
770 ments over an urban area based on two towers. *Atmospheric Measurement*  
771 *Techniques*, *11*(10), 5421–5438.
- 772 Jongen, H. J., Steeneveld, G.-J., Beringer, J., Christen, A., Chrysoulakis, N., Fortu-  
773 niak, K., ... Teuling, R. (2022). Urban water storage capacity inferred from  
774 observed evapotranspiration recession. *Geophysical Research Letters*, *49*(3),  
775 e2021GL096069.
- 776 Karsisto, P., Fortelius, C., Demuzere, M., Grimmond, C. S. B., Oleson, K.,  
777 Kouznetsov, R., ... Järvi, L. (2016). Seasonal surface urban energy bal-  
778 ance and wintertime stability simulated using three land-surface models in  
779 the high-latitude city Helsinki. *Quarterly Journal of the Royal Meteorological*  
780 *Society*, *142*(694), 401–417.
- 781 Klaassen, W., Bosveld, F., & De Water, E. (1998). Water storage and evaporation as  
782 constituents of rainfall interception. *Journal of Hydrology*, *212*, 36–50.
- 783 Kokkonen, T., Grimmond, C. S. B., Christen, A., Oke, T., & Järvi, L. (2018).  
784 Changes to the water balance over a century of urban development in two  
785 neighborhoods: Vancouver, Canada. *Water Resources Research*, *54*(9), 6625–

- 786 6642.
- 787 Koopmans, S., Heusinkveld, B., & Steeneveld, G. (2020). A standardized physical  
788 equivalent temperature urban heat map at 1-m spatial resolution to facili-  
789 tate climate stress tests in the Netherlands. *Building and Environment*, *181*,  
790 106984.
- 791 Kotthaus, S., & Grimmond, C. S. B. (2014a). Energy exchange in a dense urban  
792 environment—part II: Impact of spatial heterogeneity of the surface. *Urban Cli-  
793 mate*, *10*, 281–307.
- 794 Kotthaus, S., & Grimmond, C. S. B. (2014b). Energy exchange in a dense urban  
795 environment—part I: Temporal variability of long-term observations in central  
796 London. *Urban Climate*, *10*, 261–280.
- 797 Kowalczyk, E., Wang, Y., Law, R., Davies, H., McGregor, J., & Abramowitz, G.  
798 (2006). The CSIRO Atmosphere Biosphere Land Exchange (CABLE) model  
799 for use in climate models and as an offline model. *CSIRO Marine and Atmo-  
800 spheric Research Paper*, *13*, 42.
- 801 Krayenhoff, E. S., & Voogt, J. A. (2007). A microscale three-dimensional urban en-  
802 ergy balance model for studying surface temperatures. *Boundary-Layer Meteo-  
803 rology*, *123*(3), 433–461.
- 804 Kusaka, H., Kondo, H., Kikegawa, Y., & Kimura, F. (2001). A simple single-layer  
805 urban canopy model for atmospheric models: Comparison with multi-layer and  
806 slab models. *Boundary-Layer Meteorology*, *101*(3), 329–358.
- 807 Lavoisier, A. L. (1789). *Traite elementaire de chimie*. Paris.
- 808 Lemonsu, A., Viguie, V., Daniel, M., & Masson, V. (2015). Vulnerability to heat  
809 waves: Impact of urban expansion scenarios on urban heat island and heat  
810 stress in Paris (France). *Urban Climate*, *14*, 586–605.
- 811 Leopold, L. B. (1968). *Hydrology for urban land planning: A guidebook on the hydro-  
812 logic effects of urban land use* (Vol. 554). US Geological Survey.
- 813 Lipson, M. J., & Best, M. (2022). *Benchmarks for the urban-plumber model evalua-  
814 tion project phase 1 (au-preston) (versie v1) [data set]*. Zenodo. doi: [https://  
815 doi.org/10.5281/zenodo.7330052](https://doi.org/10.5281/zenodo.7330052)
- 816 Lipson, M. J., Grimmond, C. S. B., Best, M., Abramowitz, G., Coutts, A., Tapper,  
817 N., ... Pitman, A. J. (2023a). Evaluation of 30 urban land surface models in  
818 the Urban-PLUMBER project: Phase 1 results. *Quarterly Journal of the Royal  
819 Meteorological Society*.
- 820 Lipson, M. J., Grimmond, C. S. B., Best, M., Chow, W. T., Christen, A.,  
821 Chrysoulakis, N., ... others (2022b). *Site data archive for "harmonized gap-  
822 filled dataset from 20 urban flux tower sites" for the Urban-PLUMBER project  
823 (version v1) [data set]*. Zenodo. doi: <https://doi.org/10.5281/zenodo.2525662>
- 824 Lipson, M. J., Grimmond, C. S. B., Best, M. J., Chow, W. T., Christen, A.,  
825 Chrysoulakis, N., ... others (2022a). Harmonized gap-filled datasets from  
826 20 urban flux tower sites. *Earth System Science Data Discussions*, 1–29.
- 827 Lipson, M. J., Grimmond, S., Best, M., Abramowitz, G., Coutts, A., Tapper, N.,  
828 ... Wang, Z.-H. (2023b). The Urban-PLUMBER model evaluation project:  
829 Phase 1 results. Sydney, Australia. (11<sup>th</sup> International Conference on Urban  
830 Climate)
- 831 Lipson, M. J., Thatcher, M., Hart, M. A., & Pitman, A. (2018). A building energy  
832 demand and urban land surface model. *Quarterly Journal of the Royal Meteo-  
833 rological Society*, *144*(714), 1572–1590.
- 834 MacKay, M. D., Meyer, G., & Melton, J. R. (2022). On the discretization of  
835 Richards equation in Canadian land surface models. *Atmosphere-Ocean*, 1–  
836 11.
- 837 Manabe, S. (1969). Climate and the ocean circulation: I. the atmospheric circulation  
838 and the hydrology of the earth's surface. *Monthly Weather Review*, *97*(11),  
839 739–774.
- 840 Masson, V., Gomes, L., Pigeon, G., Lioussé, C., Pont, V., Lagouarde, J.-P., ... oth-

- 841 ers (2008). The canopy and aerosol particles interactions in Toulouse urban  
 842 layer (CAPITOU) experiment. *Meteorology and Atmospheric Physics*, *102*,  
 843 135–157.
- 844 Mauder, M., Foken, T., & Cuxart, J. (2020). Surface-energy-balance closure over  
 845 land: a review. *Boundary-Layer Meteorology*, *177*(2), 395–426.
- 846 McNorton, J., Arduini, G., Bousseres, N., Agustí-Panareda, A., Balsamo, G., Bous-  
 847 setta, S., ... Hogan, R. (2021). An urban scheme for the ECMWF integrated  
 848 forecasting system: Single-column and global offline application. *Journal of*  
 849 *Advances in Modeling Earth Systems*, e2020MS002375.
- 850 Meili, N., Manoli, G., Burlando, P., Bou-Zeid, E., Chow, W. T., Coutts, A. M., ...  
 851 others (2020). An urban ecohydrological model to quantify the effect of veg-  
 852 etation on urban climate and hydrology (UT&C v1. 0). *Geoscientific Model*  
 853 *Development*, *13*(1), 335–362.
- 854 Menzer, O., & McFadden, J. P. (2017). Statistical partitioning of a three-year time  
 855 series of direct urban net CO<sub>2</sub> flux measurements into biogenic and anthro-  
 856 pogenic components. *Atmospheric Environment*, *170*, 319–333.
- 857 Mitchell, V. G., Mein, R. G., & McMahon, T. A. (2001). Modelling the urban water  
 858 cycle. *Environmental Modelling & Software*, *16*(7), 615–629.
- 859 Morin, E., Enzel, Y., Shamir, U., & Garti, R. (2001). The characteristic time scale  
 860 for basin hydrological response using radar data. *Journal of Hydrology*, *252*(1-  
 861 4), 85–99.
- 862 Nachtergaele, F. (2001). Soil taxonomy—a basic system of soil classification for mak-  
 863 ing and interpreting soil surveys. *Geoderma*, *99*(3-4), 336–337.
- 864 Nordbo, A., Järvi, L., Haapanala, S., Moilanen, J., & Vesala, T. (2013). Intra-city  
 865 variation in urban morphology and turbulence structure in Helsinki, Finland.  
 866 *Boundary-Layer Meteorology*, *146*, 469–496.
- 867 Oke, T. R. (1982). The energetic basis of the urban heat island. *Quarterly Journal*  
 868 *of the Royal Meteorological Society*, *108*(455), 1–24.
- 869 Oleson, K. W., Bonan, G. B., Feddema, J., Vertenstein, M., & Grimmond, C. S. B.  
 870 (2008). An urban parameterization for a global climate model. part I: For-  
 871 mulation and evaluation for two cities. *Journal of Applied Meteorology and*  
 872 *Climatology*, *47*(4), 1038–1060.
- 873 Oleson, K. W., & Feddema, J. (2020). Parameterization and surface data improve-  
 874 ments and new capabilities for the community land model urban (CLMU).  
 875 *Journal of advances in modeling earth systems*, *12*(2), e2018MS001586.
- 876 Pawlak, W., Fortuniak, K., & Siedlecki, M. (2011). Carbon dioxide flux in the centre  
 877 of Łódź, poland—analysis of a 2-year eddy covariance measurement data set.  
 878 *International Journal of Climatology*, *31*(2), 232–243.
- 879 Peters, E. B., Hiller, R. V., & McFadden, J. P. (2011). Seasonal contributions of  
 880 vegetation types to suburban evapotranspiration. *Journal of Geophysical Re-*  
 881 *search: Biogeosciences*, *116*(G1).
- 882 Petrucci, R. H., Herring, F. G., & Madura, J. D. (2010). *General chemistry: princi-*  
 883 *ples and modern applications*. Pearson Prentice Hall.
- 884 Porson, A., Clark, P. A., Harman, I., Best, M. J., & Belcher, S. (2010). Implemen-  
 885 tation of a new urban energy budget scheme in the metum. part I: Description  
 886 and idealized simulations. *Quarterly Journal of the Royal Meteorological Soci-*  
 887 *ety*, *136*(651), 1514–1529.
- 888 Randrup, T. B., McPherson, E. G., & Costello, L. R. (2001). Tree root intrusion in  
 889 sewer systems: A review of extent and costs. *Journal of Infrastructure Systems*  
 890 *7: 26-31*, *7*, 26–31.
- 891 Ronda, R., Steeneveld, G., Heusinkveld, B., Attema, J., & Holtslag, A. (2017). Ur-  
 892 ban finescale forecasting reveals weather conditions with unprecedented detail.  
 893 *Bulletin of the American Meteorological Society*, *98*(12), 2675–2688.
- 894 Ross, S. L., & Oke, T. (1988). Tests of three urban energy balance models.  
 895 *Boundary-Layer Meteorology*, *44*(1), 73–96.

- 896 Roth, M., Jansson, C., & Velasco, E. (2017). Multi-year energy balance and carbon  
897 dioxide fluxes over a residential neighbourhood in a tropical city. *International*  
898 *Journal of Climatology*, *37*(5), 2679–2698.
- 899 Ryu, Y.-H., Baik, J.-J., & Lee, S.-H. (2011). A new single-layer urban canopy model  
900 for use in mesoscale atmospheric models. *Journal of Applied Meteorology and*  
901 *Climatology*, *50*(9), 1773–1794.
- 902 Sadegh, M., AghaKouchak, A., Flores, A., Mallakpour, I., & Nikoo, M. R. (2019).  
903 A multi-model nonstationary rainfall-runoff modeling framework: analysis and  
904 toolbox. *Water Resources Management*, *33*(9), 3011–3024.
- 905 Saxton, K., Rawls, W., Romberger, J. S., & Papendick, R. (1986). Estimating gen-  
906 eralized soil-water characteristics from texture. *Soil Science Society of America*  
907 *Journal*, *50*(4), 1031–1036.
- 908 Schulz, J.-P., & Vogel, G. (2020). Improving the processes in the land surface  
909 scheme TERRA: Bare soil evaporation and skin temperature. *Atmosphere*,  
910 *11*(5), 513.
- 911 Shuster, W. D., Bonta, J., Thurston, H., Warnemuende, E., & Smith, D. (2005). Im-  
912 pacts of impervious surface on watershed hydrology: A review. *Urban Water*  
913 *Journal*, *2*(4), 263–275.
- 914 Stagakis, S., Chrysoulakis, N., Spyridakis, N., Feigenwinter, C., & Vogt, R. (2019).  
915 Eddy covariance measurements and source partitioning of CO<sub>2</sub> emissions in an  
916 urban environment: Application for heraklion, greece. *Atmospheric Environ-*  
917 *ment*, *201*, 278–292.
- 918 Steeneveld, G.-J., van der Horst, S., & Heusinkveld, B. (2020). Observing the sur-  
919 face radiation and energy balance, carbon dioxide and methane fluxes over  
920 the city centre of Amsterdam. In *EGU general assembly conference abstracts*  
921 (p. 1547).
- 922 Stewart, I. D., & Oke, T. R. (2012). Local climate zones for urban temperature  
923 studies. *Bulletin of the American Meteorological Society*, *93*(12), 1879–1900.
- 924 Sun, R., Wang, Y., & Chen, L. (2018). A distributed model for quantifying  
925 temporal-spatial patterns of anthropogenic heat based on energy consump-  
926 tion. *Journal of Cleaner Production*, *170*, 601–609.
- 927 Templeton, N. P., Vivoni, E. R., Wang, Z.-H., & Schreiner-McGraw, A. P. (2018).  
928 Quantifying water and energy fluxes over different urban land covers in  
929 phoenix, arizona. *Journal of Geophysical Research: Atmospheres*, *123*(4),  
930 2111–2128.
- 931 Tewari, M., Chen, F., Kusaka, H., & Miao, S. (2007). Coupled WRF/Unified  
932 Noah/urban-canopy modeling system. In *Ncar WRF documentation, NCAR,*  
933 *Boulder* (Vol. 122, pp. 1–22). Citeseer.
- 934 Thatcher, M., & Hurley, P. (2012). Simulating australian urban climate in a  
935 mesoscale atmospheric numerical model. *Boundary-Layer Meteorology*, *142*(1),  
936 149–175.
- 937 Twine, T. E., Kustas, W., Norman, J., Cook, D., Houser, P., Meyers, T., . . . Wesely,  
938 M. (2000). Correcting eddy-covariance flux underestimates over a grassland.  
939 *Agricultural and forest meteorology*, *103*(3), 279–300.
- 940 United Nations. (2018). *World urbanization prospects, the 2018 revision*. UN De-  
941 partment of Economic and Social Affairs.
- 942 Velasco, E., Perrusquia, R., Jiménez, E., Hernández, F., Camacho, P., Rodríguez, S.,  
943 . . . Molina, L. (2014). Sources and sinks of carbon dioxide in a neighborhood  
944 of Mexico City. *Atmospheric Environment*, *97*, 226–238.
- 945 Velasco, E., Pressley, S., Grivicke, R., Allwine, E., Molina, L. T., & Lamb, B.  
946 (2011). Energy balance in urban Mexico City: observation and parameteri-  
947 zation during the MILAGRO/MCMA-2006 field campaign. *Theoretical and*  
948 *applied climatology*, *103*, 501–517.
- 949 Vulova, S., Meier, F., Rocha, A. D., Quanz, J., Nouri, H., & Kleinschmit, B. (2021).  
950 Modeling urban evapotranspiration using remote sensing, flux footprints, and

- artificial intelligence. *Science of The Total Environment*, 786, 147293.
- 952 Wald, A. (1943). Tests of statistical hypotheses concerning several parameters when  
953 the number of observations is large. *Transactions of the American Mathemat-  
954 cal Society*, 54(3), 426–482.
- 955 Walsh, C. J., Fletcher, T. D., & Ladson, A. R. (2005). Stream restoration in urban  
956 catchments through redesigning stormwater systems: looking to the catchment  
957 to save the stream. *Journal of the North American Benthological Society*,  
958 24(3), 690–705.
- 959 Wang, C., Wang, Z.-H., & Ryu, Y.-H. (2021). A single-layer urban canopy model  
960 with transmissive radiation exchange between trees and street canyons. *Build-  
961 ing and Environment*, 191, 107593.
- 962 Wang, Y. P., Kowalczyk, E., Leuning, R., Abramowitz, G., Raupach, M. R., Pak, B.,  
963 ... Luhar, A. (2011). Diagnosing errors in a land surface model (cable) in the  
964 time and frequency domains. *Journal of Geophysical Research: Biogeosciences*,  
965 116(G1).
- 966 Wang, Z.-H., Bou-Zeid, E., & Smith, J. A. (2013). A coupled energy transport  
967 and hydrological model for urban canopies evaluated using a wireless sensor  
968 network. *Quarterly Journal of the Royal Meteorological Society*, 139(675),  
969 1643–1657.
- 970 Ward, H. C., Evans, J. G., & Grimmond, C. S. B. (2013). Multi-season eddy covari-  
971 ance observations of energy, water and carbon fluxes over a suburban area in  
972 Swindon, UK. *Atmospheric Chemistry and Physics*, 13(9), 4645–4666.
- 973 Ward, H. C., Kotthaus, S., Järvi, L., & Grimmond, C. S. B. (2016). Surface urban  
974 energy and water balance scheme (SUEWS): development and evaluation at  
975 two UK sites. *Urban Climate*, 18, 1–32.
- 976 Wenzel Jr, H. G., & Voorhees, M. L. (1981). *Evaluation of the urban design storm  
977 concept*. University of Illinois at Urbana-Champaign. Water Resources Center.
- 978 Willmott, C. J. (1982). Some comments on the evaluation of model performance.  
979 *Bulletin of the American Meteorological Society*, 63(11), 1309–1313.
- 980 WMO. (2019). *Guidance on integrated urban hydrometeorological, climate and envi-  
981 ronmental services - volume i*. Geneva.
- 982 Wouters, H., Demuzere, M., De Ridder, K., & van Lipzig, N. P. (2015). The impact  
983 of impervious water-storage parametrization on urban climate modelling. *Ur-  
984 ban Climate*, 11, 24–50.
- 985 Yang, Z.-L., Dickinson, R., Henderson-Sellers, A., & Pitman, A. (1995). Preliminary  
986 study of spin-up processes in land surface models with the first stage data of  
987 project for intercomparison of land surface parameterization schemes phase 1  
988 (a). *Journal of Geophysical Research: Atmospheres*, 100(D8), 16553–16578.
- 989 Yao, L., Wei, W., & Chen, L. (2016). How does imperviousness impact the urban  
990 rainfall-runoff process under various storm cases? *Ecological indicators*, 60,  
991 893–905.
- 992 Yu, M., Wu, H., Yin, J., Liang, X., & Miao, S. (2022). Improved delineation of  
993 urban hydrological processes in coupled regional climate models. *Water Re-  
994 sources Research*, e2022WR032695.
- 995 Zeisl, P., Mair, M., Kastlunger, U., Bach, P. M., Rauch, W., Sitzenfrie, R., & Klei-  
996 dorfer, M. (2018). Conceptual urban water balance model for water policy  
997 testing: an approach for large scale investigation. *Sustainability*, 10(3), 716.
- 998 Zhou, Q., Leng, G., Su, J., & Ren, Y. (2019). Comparison of urbanization and  
999 climate change impacts on urban flood volumes: Importance of urban planning  
1000 and drainage adaptation. *Science of the Total Environment*, 658, 24–33.